Scanning Microscopy

Volume 1990
Number 4 *Fundamental Electron and Ion Beam Interactions with Solids for Microscopy, Microanalysis, and Microlithography*

Article 7

1990

Secondary Electron Emission from Solids. II. Theoretical Descriptions

Michel Cailler
Université de Nantes, France

Jean-Pierre Ganachaud
Université de Nantes, France

Follow this and additional works at: https://digitalcommons.usu.edu/microscopy

Part of the Biology Commons

Recommended Citation

Cailler, Michel and Ganachaud, Jean-Pierre (1990) "Secondary Electron Emission from Solids. II. Theoretical Descriptions," *Scanning Microscopy*: Vol. 1990 : No. 4 , Article 7.
Available at: https://digitalcommons.usu.edu/microscopy/vol1990/iss4/7

This Article is brought to you for free and open access by the Western Dairy Center at DigitalCommons@USU. It has been accepted for inclusion in Scanning Microscopy by an authorized administrator of DigitalCommons@USU. For more information, please contact digitalcommons@usu.edu.

Scanning Microscopy Supplement 4, 1990 (Pages 81-110) 0892-953X/90$3.00+.00
Scanning Microscopy International, Chicago (AMF O'Hare), IL 60666 USA

SECONDARY ELECTRON EMISSION FROM SOLIDS. II. THEORETICAL DESCRIPTIONS

Michel Cailler[1]* and Jean-Pierre Ganachaud[2]

[1] ISITEM de l'Université de Nantes, Laboratoire de Sciences des Surfaces et Interfaces en Mécanique, 44087 Nantes Cédex 03, France.
[2] Faculté des Sciences et Techniques de l'Université de Nantes, Laboratoire de Physique du Solide Théorique, 2 Rue de la Houssinière, 44072 Nantes Cedex, France

Abstract

A primary beam impinging on a solid target suffers elastic and inelastic collisions with the components of the solid. These collisions can be incorporated into a Monte-Carlo simulation model if all the cross sections associated with the various types of collisions are known.

Elastic diffusion effects are mainly related to the interactions of the particles with the real potential V(r) surrounding each ionic core. An essential simplification of the inelastic interactions is to consider that the solid reacts as a whole to an external probe, which is the incident electron beam. The linear response of the solid to an external perturbation is described by its dielectric function

In the present paper, the methods used to evaluate the elastic and inelastic cross-sections and to simulate the secondary electron emission are reviewed and discussed.

Key Words: Electron-induced secondary electron emission, elastic collisions, inelastic collisions, partial wave analysis, first Born approximation, screened Rutherford scattering cross-section, Lindhard dielectric function, individual transi-tions, plasmon decay, Gryzinski's inner-shell cross-sections, Monte-Carlo simulation method, layer-by-layer model, Boltzmann transport equation, energy distributions, yields.

* Address for correspondance:
Michel Cailler
ISITEM de l'Université de Nantes
Laboratoire de Sciences des Surfaces et Interfaces en Mécanique
La Chantrerie CP 3023, 44087
Nantes Cédex 03
France
Phone No 40291616

1) Introduction

A primary beam impinging on a solid target suffers elastic and inelastic collisions with the components of the solid. The effect of the inelastic collisions is to bring the electrons of the solid to upper energy levels so that they can themselves take part in the transport process. This is the cascade effect. In a study of the secondary electron emission, one must a priori describe precisely all the collisions that are caused by the primary electrons which penetrate the target or those that are elastically turned back towards the surface. In addition, one must follow all the electrons of the cascade which maintain an energy above the vacuum level, that is the inelastically backscattered primaries and the secondary electrons. These latter can be produced in one of the emission mechanisms we described in part I: direct transition from an ionic core level or from the valence band to an unoccupied level above the vacuum level, Auger transition, plasmon decay and autoionization emission. All the excitation processes occuring with a reasonable probability in a given material must be incorporated in a rigorous theoretical description of the secondary electron emissive properties of this material. They can be incorporated, a priori easily, into a Monte-Carlo simulation. However, this is not often the case and for instance autoionization emission has never been taken into account in quantitative descriptions of the secondary electron emission. Practically, it can be considered that rather rigorous theoretical treatments have only been developed in the case of normal metals, especially for Al. In the simulation of the secondary electron emission, the need of following all the electrons of the cascade down to the vacuum level renders the technique expensive in computer time and in money. The access to cheaper microcomputers and the development of more efficient methods should allow a

larger extension of the technique. Alternatively, the excitation processes can also be incorporated into a Boltzmann transport equation. But again, in order to obtain a realistic and complete description of the secondary electron emission, usually a long computer time is needed.

2) Elastic collisions

Elastic diffusion effects are mainly related to the interactions of the particles with the real potential V(r) surrounding each ionic core. Various approximations for the potential and different techniques of calculations have been proposed to evaluate the elastic cross-sections. They are reviewed and discussed in what follows.

2.1. Techniques of calculations.

2.1.1. partial wave analysis (PWA). The differential elastic cross section can be given by a partial wave analysis as (see for instance, Cailler *et al.* (1983)):

$$K^{-2}\left[\sum_{l=0}^{\infty}(2l+1)\exp(i\delta_l)\sin\delta_l P_l(\cos\theta)\right]^2 \quad (1)$$

where K is the wave number of the incident electron, $P_l(\cos\theta)$ is the l-order Legendre polynomial and δ_l is the phase-shift suffered by the lth partial wave. The total elastic cross section is:

$$\sigma_{el}(E) = 2\pi\int_0^{\pi}\sin\theta\, d\theta\, \sigma_{el}(E,\theta)$$

$$= 4\pi K^{-2}\sum_{l=0}^{\infty}(2l+1)\sin^2\delta_l \quad (2)$$

and the elastic mean free path $\lambda_e(E)$ can be written:

$$\lambda_e(E) = [N_{at}\,\sigma_{el}(E)]^{-1} \quad (3)$$

where N_{at} stands for the number of atoms per unit volume.

A similar partial wave expansion method including relativistic effects was used by Ichimura and Shimizu (1981) under the form:

$$\frac{d\sigma_{el}(\theta)}{d\theta} = |f(\theta)|^2 + |g(\theta)|^2 \quad (4)$$

with:

$$f(\theta) = \frac{1}{2iK}\sum_{l=0}^{\infty}\Big\{(l+1)\left[\exp(2i\eta_l)-1\right] + l\left[\exp(2i\eta_{-l-1})-1\right]P_l(\cos\theta)\Big\} \quad (5)$$

and:

$$g(\theta) = \frac{1}{2iK}\sum_{l=1}^{\infty}\left[-\exp(2i\eta_l)+\exp(2i\eta_{-l-1})\right] P_l^1(\cos\theta) \quad (6)$$

In these relations η_l is the appropriate phase-shift and $P_l(\cos\theta)$ and $P_l^1(\cos\theta)$ the lth Legendre and associated Legendre function, respectively. The phase-shifts completely determine the scattering and they can be evaluated when the scattering potential is known. Details of calculations can be found in Ichimura and Shimizu's papers or in a recent paper by Jablonski et al. (1989).

2.1.2. First Born approximation. In this method the unperturbed state of the incident electron is a plane wave function and the potential energy of interaction between the incident electron and the scattering center is regarded as a perturbation of this unperturbed plane wave function. The scattered wave is usually calculated only to first order in the scattering potential. This is the first Born approximation. The validity of the first Born approximation was analyzed by Schiff (1955) who showed that this perturbation treatment is most useful for high energies and therefore could be a supplement to the method of partial waves. An additional restrictive argument on the validity of the first Born approximation can be found in Schiff's book in which the diffusion by a square well is studied. It is shown that the method gives good results in the case of a narrow well and that its validity is weakened as the width of the well is increased. Extending the argument to atoms, it can be expected that the approximation does not work well for large atoms.

2.1.3. Screened Rutherford scattering formula. The screened Rutherford scattering cross-section is an example of the application of the Born approximation. It was derived from a Wentzel screened coulombic potential, which can be written:

$$V(r) = -\frac{1}{4\pi\varepsilon_0}\frac{Ze^2}{r}\exp\left(-\frac{r}{\rho_s}\right) \quad (7)$$

where Z is the atomic number, e the electronic charge, ε_0 the vacuum permittivity and ρ_s the screening radius. The coulombic potential is obtained by neglecting the screening effects and corresponds to an infinite value of ρ_s.

With the screened potential, the differential cross-section per unit volume and solid angle element is :

$$\frac{d\sigma_{el}}{d\Omega} = \frac{1}{(4\pi\varepsilon_0)^2} N_{at} \frac{Z^2 e^4}{4E^2} \frac{1}{(1+2\beta-\cos\theta)^2} \quad (8)$$

and the total cross-section is :

$$\sigma_{el}(E) = \int_{\Omega_{tot}} d\Omega \frac{d\sigma_{el}}{d\Omega} = \frac{1}{(4\pi\varepsilon_0)^2} N_{at} \frac{Z^2 e^4}{4E^2} \frac{\pi}{\beta(1+\beta)} \quad (9)$$

In these relations, N_{at} stands for the number of atoms per unit volume, E for the electron energy, θ for the scattering angle and the parameter β accounts for the screening of the nuclear charge by the orbital electrons. A relativistic version of the differential elastic cross-section can be obtained by multiplying the above non-relativistic expression of $d\sigma_{el} / d\Omega$ by a spin-relativistic correction factor. Both versions were used by Berger *et al.* (1970) in a pioneering work on the simulation of the spatial distribution of the energy deposited by electrons in the atmosphere.

The parameter β is connected with ρ_s by the relation :

$$\beta = \frac{\hbar^2}{8\,m\,E} \rho_s^{-2} \quad (10)$$

According to the Thomas-Fermi statistical theory of atoms (see for instance Schiff (1955)), the "radius" ρ_s of the atomic electron cloud that screens the nucleus can be taken as being :

$$\rho_s = \rho_{TF} \equiv \frac{1}{2}\left(\frac{3\pi}{4}\right)^{2/3} a_0 (Z)^{-1/3} \simeq 0.885\ a_0 (Z)^{-1/3} \quad (11)$$

In that case $\beta = 4.34 \frac{Z^{2/3}}{E}$ if E is measured in eV. This relation was recently used by Werner and Heydenreich (1984) in a study of the electron transmission and backscattering with a multiple collision model. Some other approximations of the screening radius have also been considered. For instance, Tholomier *et al.* (1987, 1988) used the screened Rutherford cross section in the Lenz's approximation of the screening radius: $\rho_s = a_0\ Z^{-1/3}$.

Shimizu *et al.* (1972) and Ichimura and Shimizu (1981) used for the screening parameter β an expression given by Nigam et al. (1959):

$$\beta = \frac{\hbar^2}{8\,m\,E}\ 1.12^2\ \rho_{TF}^{-2} = 5.44\ \frac{Z^{2/3}}{E} \quad (12)$$

if E is measured in eV. For the screening radius, this is equivalent to take

$$\rho_s = \frac{\rho_{TF}}{1.12} \quad (13)$$

Some other expressions were proposed for the screening parameter β. For instance, Adesida *et al.* (1978) used half the value of the screening parameter as calculated by the above relation and Jousset (1987a) took $\beta = 2.61\ Z^{2/3}/E$.

2.2. *Discussion*

2.2.1. Choice of the potential. In order to get right values of the elastic cross-section, one has to adopt a potential which has to be as exact as possible. For Al, Ganachaud and Cailler (1979a) used a muffin-tin potential evaluated by Smrcka (1970) by superposing the potentials of the different ionic sites and by using a Slater exchange term. Ichimura and Shimizu (1981) used to evaluate the phase-shifts an analytical expression developed by Bonham and Strand (1963) to describe the potentials of neutral Thomas-Fermi-Dirac atoms, that is:

$$V(r) = -\frac{1}{4\pi\varepsilon_0} \frac{Z e^2}{r} \sum_{i=1}^{3} \gamma_i \exp(-\lambda_i r) \quad (14)$$

where

$$\gamma_i = a_i + b_i (\ln Z) + c_i (\ln Z)^2 + d_i (\ln Z)^3 + e_i (\ln Z)^4 \quad (15)$$

and with equivalent expressions for the λ_i's. Values of the constants a_i, b_i, c_i, d_i and e_i for the determination of the γ_i's and λ_i's were found in Bonham and Strand (1963). For Al, Jousset (1987a) has proceeded to a comparison between the Smrcka, the Bonham and Strand and the coulombic potentials. These results, completed by the Wentzel potential are shown in Fig.1. It can be seen that differences between the values of these potentials occur at large distances, the Coulombic potential being the most deeper because it does not take into account the screening by the inner-shell electrons. The atomic potential of Bonham and Strand goes to zero when the distance r goes

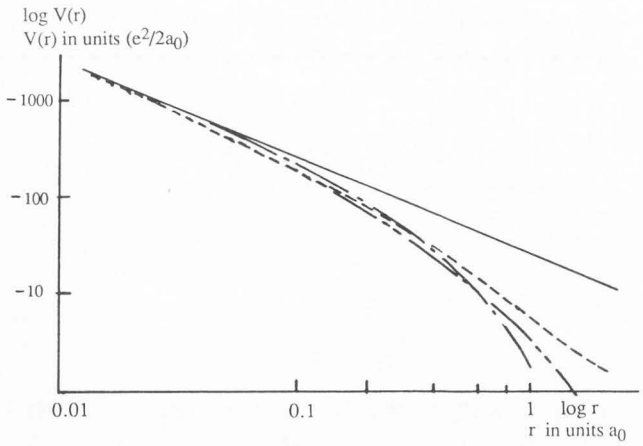

Fig.1 : Variation in the potential, as a function of the radial distance from Al nucleus (After Jousset (1987a)) (———) Coulombic potential : - (2Z)/r; (- - - - - - - -) Smrcka; (——- - ——- -) Thomas-Fermi-Dirac potential; (——- - ——- -) Wentzell screened Coulombic potential : - (2Z)/r exp(-r/ρ_S) with ρ_S=0.885 $a_0/Z^{1/3}$.

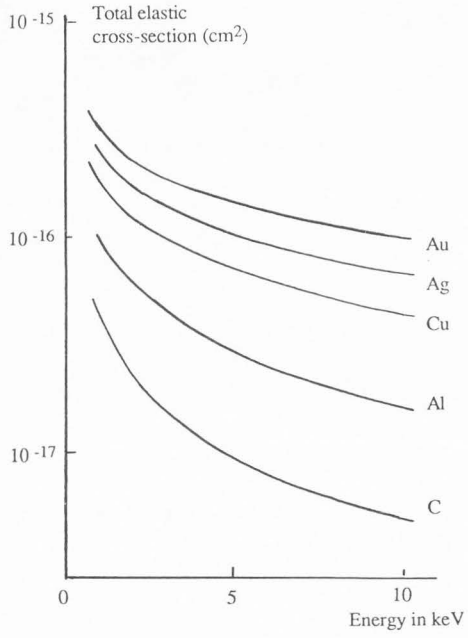

Fig.2 : Energy dependence of the total elastic cross-section of several elements (After Ichimura and Shimizu (1981)).

to infinity, whereas the Smrcka potential remains negative and practically constant outside the muffin-tin spheres. Consequently, the differences observed in the potential values at large distances induce changes in the values of the differential cross-sections, at small scattering angles, especially for lower electron energies. As shown by

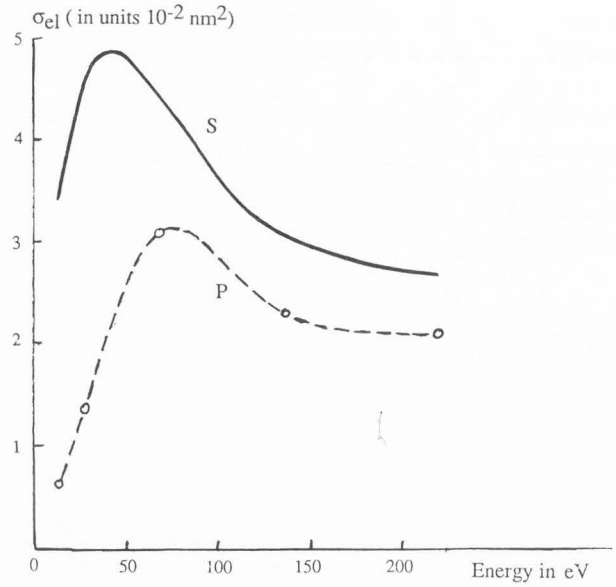

Fig. 3 : Energy dependence of the elastic cross-section calculated with two different potentials. P : Pendry's potential (1974); S : Smrcka's potential (1970).

the Bonham and Strand expression for V(r), the depth of the potential well is an increasing function of the atomic number Z. Consequently, the scattering effect of the potential, as measured by the total elastic cross-section increases with an increasing Z (see Fig.2).

It was also shown by Ganachaud (1977), that at low energies (for instance under 100 eV in Al), the elastic mean free path as given by a partial wave analysis is itself highly sensitive to the particular choice made for the potential. This was established by comparing results deduced from Smrcka's potential and from a self-consistent one calculated by Pendry (1974).

The observed discrepancies between the cross-section values (see fig.3) were attributed, to the fact that one of the potentials was self-consistently calculated and the other not, and most likely, to the nature of the exchange term. Indeed, in spite of its non-consistent nature, the Slater exchange term is considered as partially taking into account the correlation effects and therefore, as giving a better description of the solid potential.

With respect to the Thomas-Fermi-Dirac potentials Jousset (1987a) considered that they were a good approximation for heavier atoms and for not too high radial distances.

2.2.2. Choice of the technique of calculations. A comparison between the results calculated in the first Born approximation and

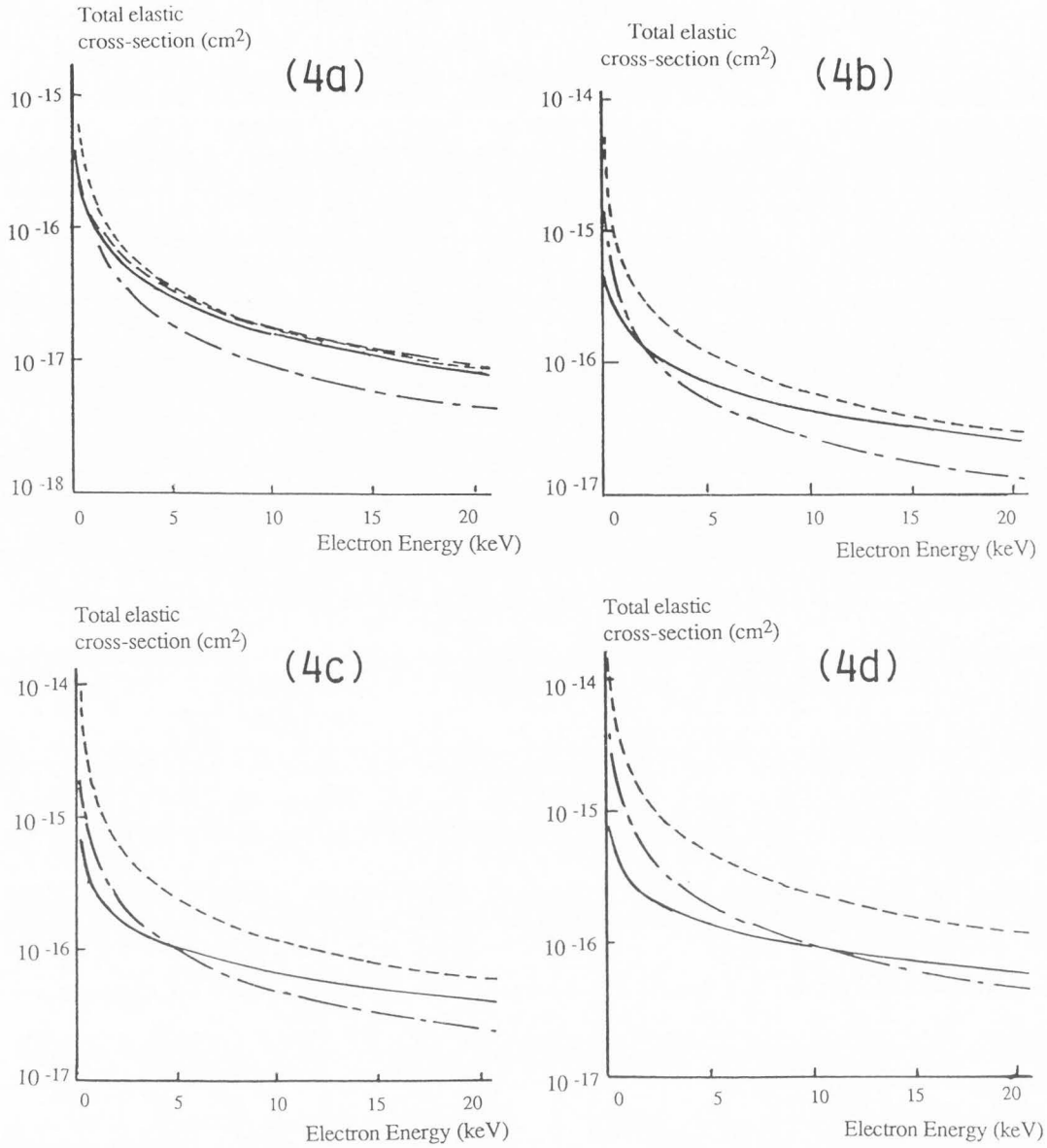

Fig. 4 : Total elastic cross-sections for Al (a), Cu (b), Ag (c) and Au (d) (From Ichimura and Shimizu (1981).
(————————) Partial wave analysis and Thomas-Fermi potential,
(— — — — — —) Partial wave analysis and Hartree-Fock potential,
(- - - - - - - -) First Born approximation and Thomas-Fermi potential,
(—— - —— -) Screened Rutherford cross-section.

those obtained by using the PWA was performed by Ichimura and Shimizu (1981) and by Jousset (1987a). For Al, a close agreement was obtained between PWA and the first Born approximation in a large energy range (up to keV). But, for heavy atoms, Ichimura and Shimizu observed that the first Born approximation could no longer give results close to those obtained by the PWA, the difference becoming larger as the atomic number of the target atom increased (Fig.4). They have considered that this was probably caused by fine features appearing in the differential cross-sections given by the PWA approach and not in those calculated in the first Born approximation. In that latter case, only a smooth variation of the differential cross-section with the scattering angle was observed. Such fine features were becoming more important for heavy atoms. Restrictions in the use of the first Born approximations are not surprising if considerations on the electron energy

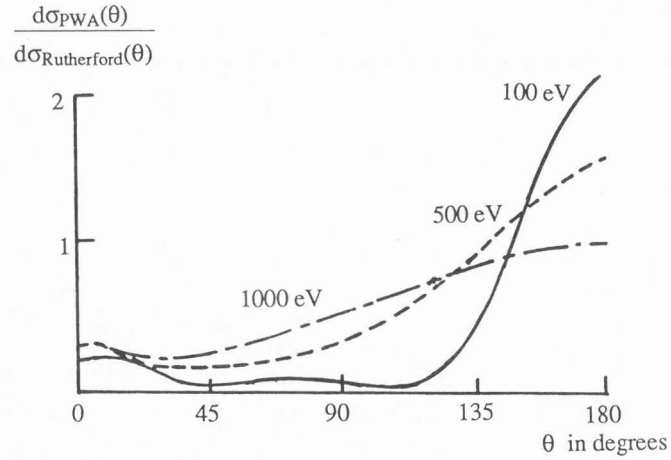

Fig. 5 : Ratio of the angle-dependent differential elastic cross-section in Al, for different primary energies.

and the width of the well as developed by Schiff (1955) are taken into account.

Ichimura and Shimizu (1981) and Jousset (1987a) have also proceeded to a comparison between the cross-sections obtained with the two above methods and a screened Rutherford scattering cross-section. Ichimura and Shimizu (1981) used for the screening parameter β the expression as given by Nigam *et al.* (1959). They observed that the cross-sections obtained by the screened Rutherford formula differed from those obtained by the PWA or the first Born approximation, even for Al (Fig.4). According to Jousset (1987a) the total elastic cross-section evaluated in Al, with a screening parameter $\beta = 2.61\ Z^{2/3}/E$, differed by 40 % at 1 keV, from the PWA results (Fig.5). Furthermore, the differential cross-section obtained was very different from that obtained by the PWA method, especially at lower energies. He suggested to multiply the Rutherford cross-section by an adjustable parameter α.

Fitting and Reinhardt (1985) used for the elastic cross-section a PWA-fitted screened Rutherford scattering with :

$$\rho_s = \frac{0.885}{\tau}\, a_0 (Z)^{-1/3} \qquad (16)$$

In this expression, τ was an adjustable screening parameter. For high energies, τ was nearly equal to unity, but with decreasing energy E, it was corrected according to the relation :

$$\tau(E) = 0.9 + \exp(-E/E_\tau) \qquad (17)$$

where E_τ was an adjustement parameter. According to Fitting and Reinhardt nearly satisfactory values of the cross-sections were obtained with the following parameters (in eV):

	C	O	Al	Cu	Ag	Au
E_τ	350	300	250	1600	2500	7600

They proposed also to take into account the residual deviations by an additional parameter in the screened Rutherford formula.

2.2.3. Conclusion. As a conclusion of this section we want to notice that attention must be paid to the potential and the method of calculation used to evaluate the elastic cross-section. In fact, in a description of the secondary electron emission, a as precise as possible description of the potential is required. This was the justification of the choice of Smrcka's potential made by Ganachaud and Cailler for Al. If low energy (≤100 eV) electrons have to be considered, a free atom approximation for the potential could not be sufficiently precise. A better choice lies in a self-consistent potential which takes into account the redistribution of the charges coming from the delocalization of the outer shell electrons. From this point of view, the spherically symmetrical muffin-tin approximation is a very useful form. Evidently, the choice is less important if low energy electrons are not to be described. For instance, the Bonham and Strand potential works well for a study at high energies as the evaluation of the electron backscattering effects carried out by Ichimura and Shimizu.

The first Born approximation is to be used with precaution and likely not for heavy atoms. The screened Rutherford formula does not work well, especially at lower energies, except may be if adjustable supplementary parameters are introduced into the formula. But, in that latter case, the problem is transferred on the correct choice of these parameters. In the PWA method, the summation on the phase-shift has to be performed on a sufficiently large number of partial waves. On the opposite case, some accuracy losses can occur in the differential cross-section values.

3) Inelastic collisions.

3.1.The dielectric theory

A rigorous description of the inelastic interactions would be rather sophisticated. In fact, it is a many-body problem that includes all the electrons of the incident beam and of the target. An essential simplification of this problem is to consider that the solid reacts as a whole to an external probe, which is here the incident electron beam. The dielectric theory of the response of the

solid can be regarded as having a sufficiently general frame (see for instance, Ganachaud and Cailler (1979a)). The probability for an electron to transfer an energy $\hbar\omega$ and a momentum $\hbar q$ to an electron of the metal is :

$$\phi(q,\omega) = \frac{1}{q}\ \mathrm{Im}\left\{-\frac{1}{[\varepsilon(q,\omega)]}\right\} \qquad (18)$$

3.1.1. Random-phase approximation in an infinite electron gas. In the random-phase approximation, the linear response of an infinite electron gas to an external perturbation is given by the Lindhard dielectric function $\varepsilon(q,\omega)$. This is a complex quantity:

$$\varepsilon = \varepsilon_1 + i\,\varepsilon_2 \qquad (19)$$

which in fact depends only on the modulus q of $\vec{q}$. According to Lindhard (1954) :

$$\varepsilon_1 = 1 + \frac{\alpha r_s}{8\pi}\frac{1}{z^3}\left[4z + f(z+u) + f(z-u)\right] \qquad (20)$$

$$\text{where: } z = \frac{q}{2k_F},\quad y = \frac{\hbar\omega}{4E_F},\quad u = \frac{y}{z}, \qquad (20')$$

$$\alpha = \left(\frac{4}{9\pi}\right)^{1/3} \text{ and } f(a) = (1-a^2)\ln\left|\frac{a+1}{a-1}\right| \qquad (20'')$$

$$\varepsilon_2 = \frac{\alpha r_s}{8\pi}\frac{1}{z^3}B(z,u) \qquad (21)$$

with :

$$B(z,u) = \left[1-(u-z)^2\right]$$

$$\text{for } \frac{\hbar^2}{2m}(q^2-2qk_F) \le \hbar\omega \le \frac{\hbar^2}{2m}(q^2+2qk_F)$$

$$\text{and } \hbar\omega \ge \frac{\hbar^2}{2m}(2qk_F - q^2) \qquad (21')$$

$$B(z,u) = 4uz \text{ for } 0 \le \hbar\omega \le \frac{\hbar^2}{2m}(2qk_F - q^2) \qquad (21'')$$

$$B(z,u) = 0 \text{ elsewhere.} \qquad (21''')$$

In these expressions, $E_F=(\hbar k_F)^2/(2m)$ is the Fermi level and $r_s a_0$ is the mean interelectronic radius defined by the relation :

$$4\pi r_s^3 a_0^3 = \frac{N}{\Omega} = n \qquad (22)$$

where n is the mean density of the valence electrons.

3.1.2. Plasmon modes. From a practical point of view, it is advisable to break the dielectric response function into several separate contributions, which makes the description easier. A remarkable feature of infinite electron gases is that they show a well-characterized collective oscillation mode, the plasmon mode. It is thus possible to consider in such infinite electron gases two different types of collisions, those leading to a plasmon creation and those leading directly to an electron-hole pair. For a bulk plasmon excitation (see Tung and Ritchie (1977) for an alternative solution):

$$\mathrm{Im}\left\{-\frac{1}{[\varepsilon(q,\omega)]}\right\} = \pi\,\delta[\varepsilon_1(q,\omega)]$$

$$= \pi\frac{\delta[\omega-\omega_{bp}(q)]}{[\partial\varepsilon_1/\partial\omega]_{\omega=\omega_{bp}(q)}} \qquad (23)$$

The bulk plasmon dispersion relation $\omega_{bp}(q)$ is obtained from :

$$\varepsilon_1(q,\omega_{bp}(q)) = 0 \quad (24') \quad \text{and} \quad \varepsilon_2 = 0 \quad (24'')$$

The dispersion curve enters the individual domain for the cut-off value $q = q_c$ such that :

$$\hbar\omega_{bp}(q_c) = \frac{\hbar^2}{2m}(q_c^2 + 2q_c k_F) \qquad (25)$$

For $q>q_c$, ε_2 is non-zero and the collective excitation is damped.

The plasmon creation rate was also evaluated by Quinn (1962), the corresponding mean free path being :

$$\lambda_{bp} = \frac{2a_0E}{\hbar\omega_{bp}}\left(\ln\frac{\sqrt{k_F^2 + \frac{2m}{h}\omega_{bp}} - k_F}{K - \sqrt{K^2 - \frac{2m}{h}\omega_{bp}}}\right)^{-1} \qquad (26)$$

3.1.3. Individual transitions. The individual transitions of the valence-electron gas are restricted in Lindhard's approximation to the domain of the (ω,q) plane where ε_2 is non-zero. For a given value of ω, the limiting values for q are given by :

$$-k_F + \sqrt{k_F^2 + \frac{2m\omega}{\hbar}} \equiv q_1 \le q \le q_2 \equiv +k_F + \sqrt{k_F^2 + \frac{2m\omega}{\hbar}} \qquad (27)$$

and the energy-loss function associated with the individual processes is given by :

$$\phi(\omega) = \int_{q_1(\omega)}^{q_2(\omega)} \frac{dq}{q}\ \mathrm{Im}\left\{-\frac{1}{[\varepsilon(q,\omega)]}\right\} \qquad (28)$$

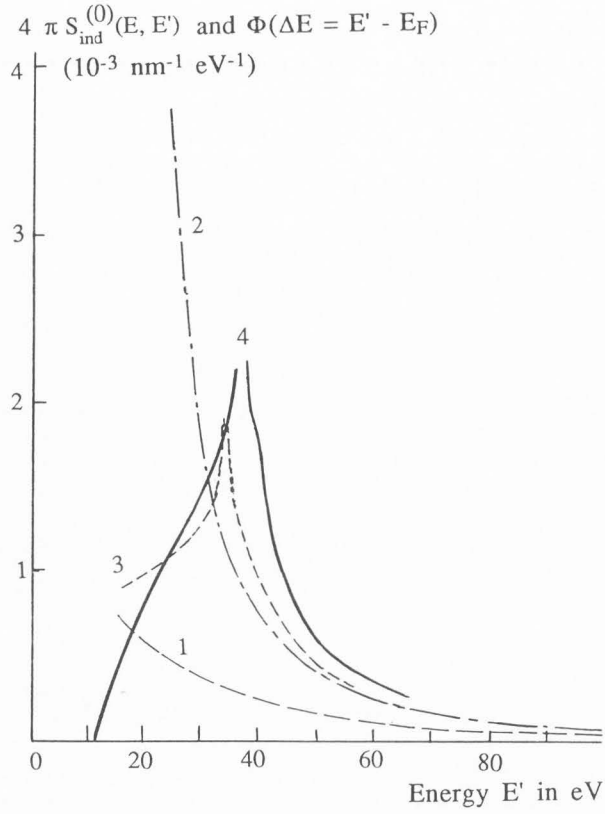

Fig.6 : Energy dependent excitation function S_C ($S_C(E, E') = 4\pi\, S_{ind}^{(0)}(E,E')$) by electron-electron scattering : Thomas-Fermi (1), unscreened (2) and Lindhard dynamical screening (3) (After Rösler and Brauer (1981b)). Energy dependent loss function $\Phi(\Delta E = E' - E_F)$ for individual collisions with the jellium (4) (After Ganachaud and Cailler (1979a)). E' is the final energy of the valence electron excited by individual collision and E is the initial energy of the energetic electron. The results for $S_C(E, E')$ were obtained for an energy E = 2 keV.

The model of the free-electron gas describes the properties of the valence band in normal metals rather well .

Shimizu and his coauthors (see for instance, Koshikawa and Shimizu (1974) and Shimizu *et al.* (1976)) described the individual excitations of the conduction band by the Streitwolf (1959) excitation function:

$$S_C(E, E') = \frac{1}{(4\pi\varepsilon_0)^2} \frac{e^4 k_F^3}{3\pi E (E'-E_F)^2} \quad \text{for } E' \geq 2.715\, E_F \qquad (29')$$

$$S_C(E, E') = \frac{1}{(4\pi\varepsilon_0)^2} \frac{0.34\, e^4 k_F^3}{3\pi E E_F^2} \quad \text{for } E_F \leq E' \leq 2.715\, E_F \qquad (29'')$$

This excitation function gives the number of secondary electrons of energy E' which are created per unit length of the path of an excited electron of energy E. In other terms, the corresponding mean free path is given by:

$$\lambda_{ind} = \left[\int_{E_F} dE'\, S_C(E, E') \right]^{-1} \qquad (30)$$

A correlation can be established between the Streitwolf excitation function and the energy-loss function $\phi(\omega)$ associated with the individual processes. Indeed, if we neglect the width of the valence band, or in other words if we assume that all the Fermi sea electrons which are promoted by the energy transfer $\hbar\omega$ have a same initial energy E_F, we can consider that the energy-loss function $\phi(\omega)$ and the Streitwolf excitation function $S_c(E, E')$ are related by :

$$\phi(\Delta E = \hbar\omega) = \phi(E' - E_F) = \pi\, a_0\, E\, S_c(E, E') \qquad (31)$$

A comparison between the values of these two functions is given in Fig. 6.

3.2. *Inner-shell excitations*

The linear response of the inner-shell electrons to an external perturbation is included in the dielectric function of the solid (but not in the Lindhard dielectric function). However, the difficulty of the quantum mechanical calculations led quite usually to use preferentially classical expressions developed by Gryzinski (1965 a,b,c) for the inner-shell cross-sections. This approximation is based on a binary collision between the incident electron of kinetic energy E and an electron of the nl subshell. In that case, the total inner shell cross-section is:

$$\sigma_{nl} = \frac{1}{(4\pi\varepsilon_0)^2} \frac{\pi e^4 z_{nl}}{E_{nl}^2} \frac{1}{U_{nl}} g(U_{nl}) \qquad (32)$$

with :

$$\frac{1}{(4\pi\varepsilon_0)^2} \pi e^4 = 6.514\ 10^{-14}\ (\text{cm})^2\ (\text{eV})^2 \qquad (33)$$

$$g(U) = \left(\frac{U-1}{U+1}\right)^{3/2} \left\{ 1 + \frac{2}{3}\left(1 - \frac{1}{2U}\right) \ln\left[e + \sqrt{U-1}\right] \right\} \qquad (34)$$

and $U_{nl} = E/E_{nl}$. In these expressions, E_{nl} is the binding energy and z_{nl} the occupation number of the nl subshell.

Shimizu and his co-authors made use of Gryzinski' formula, but they have also proposed alternative expressions to describe the inelastic

processes. For instance, Shimizu *et al.* (1975) considered in a Monte Carlo model an inelastic mean free path given by the relation $\lambda_{in}=\langle\Delta E\rangle/S$ where $\langle\Delta E\rangle$ was the mean energy loss per inelastic interaction process and S the Bethe stopping power. A probability function $f(\Delta E)$ for the electron of suffering an energy loss ΔE was proposed under the form $f(\Delta E) = (1/\Delta E)\exp(-\Delta E/\langle\Delta E\rangle)$. During an inelastic event, the moving direction of the incident electron remained unchanged.

Shimizu *et al.* (1976) have also developed a direct Monte Carlo simulation method of the electron penetration in Al. The L-shell excitation rate was described in that case, by the Gryzinski cross-section and the plasmon creation by the Quinn mean free path. In that latter mechanism, the angular deflection of the energetic electron was given as:

$$\frac{d\sigma_{bp}(\theta)}{d\theta} = \frac{1}{2\pi n a_0}\frac{\theta_E}{\theta^2+\theta_E^2} \text{ with } \theta_E = \frac{\hbar\omega_{bp}}{2E} \qquad (35)$$

3.3. Extension of Gryzinski's formulation to the valence band

Shimizu and Everhart (1978) have proposed an interesting formulation of the inelastic processes in the valence band. E_v being a mean binding energy of valence electrons, much smaller than the primary electron energy E, the total cross section for valence electron excitation was derived from an approximation of the Gryzinski equation.

$$\sigma_v(E) = \frac{1}{3}\frac{\sigma_0}{E_v}\frac{1}{T}\ln\frac{E}{E_v} \qquad (36)$$

This equation could be compared with an similar expression derived by Powell (1976) (except for a factor of 4/3) as :

$$\sigma_v(E) = \frac{\sigma_0}{E_m}\frac{1}{T}\ln\frac{4E}{E_m} \qquad (37)$$

by substituting 4 E_v for E_m.

Ritchie *et al.* (1969) have shown that the Bethe stopping power might be written as a summation of contributions from separate inelastic scatterings:

$$S_{Bethe}=S_{core}+S_{plasmon}+S_{individual}=S_{core}+S_{valence} \qquad (38)$$

Shimizu and Everhart could calculate the right-hand side of the stopping power equation:

$$S_{valence} = S_{Bethe} - S_{core} \qquad (39)$$

from Bethe's and Gryzinski's equations, respectively. Then, they introduced into their expression of $\sigma_v(E)$ an appropriate value of E_v (E_v = 4 eV) which satisfied the stopping power equation over the keV energy region. By using the relationship they had obtained between E_m and E_v (E_m = 4 E_v), Shimizu and Everhart obtained E_m = 16 eV, that is the value that Powell (1976) had proposed as the most reasonable one for aluminum.

Adesida *et al.* (1978) utilized the method proposed by Shimizu and Everhart to study the electron penetration through thin films of PMMA. Their formulation seems however very slightly different from that of the original paper, since to calculate E_v, they proposed the following relation :

$$\int_{E_v}^{E_p} d(\Delta E)\,\Delta E\,\frac{d\sigma(\Delta E)}{d(\Delta E)} = S_{Bethe} - S_{core} \qquad (40)$$

with (cf. Gryzinski):

$$\frac{d\sigma(\Delta E)}{d(\Delta E)} = \frac{\pi e^4 z_v}{(\Delta E)^3}\frac{E_v}{E_p}\left(\frac{E_p}{E_p+E_v}\right)^{3/2}\left(1-\frac{\Delta E}{E_p}\right)^{E_v/(E_v+\Delta E)}$$
$$\times\left\{\frac{\Delta E}{E_v}\left(1-\frac{E_v}{E_p}\right)+\frac{4}{3}\ln\left[2.7+\left(\frac{E_p-\Delta E}{E_v}\right)^{1/2}\right]\right\} \qquad (41)$$

and E_v = 10 eV. In the above relation, z_v is the occupancy number of the valence band.

Later, Ichimura and Shimizu (1981) have proposed a slight modification of the stopping-power equation under the form:

$$S_{valence} = S_{Bethe} - S_{core} \quad \text{for } S_{Bethe} \geq S_{core} \qquad (42')$$

and:

$$S_{valence} = 0 \quad \text{for } S_{Bethe} \leq S_{core} \qquad (42'')$$

In order to obtain the energy distribution of the backscattered electrons from aluminum, Shimizu and Ichimura (1983,1984) took into account the secondary electrons generated by the single electron excitation. They neglected, however, the generation of secondary electrons by plasmon decay as being a mechanism giving only low energy secondary electrons. For that, they described again the inelastic processes in the valence band in terms of the Quinn mean free path and the modified Streitwolf function.

A Monte-Carlo simulation technique was also developed by Valkealahti and his co-authors (1983,1984,1989) in which both core electron and valence electron excitations were described by

using Gryzinski's excitation function. The new idea was that the processes where the energy loss was smaller than the binding energy, for instance core electron excitations between two atomic levels, have to be taken into account in electron and positron slowing down.

For these processes, the excitation function was assumed to be constant and given by :

$$\frac{d\sigma(\Delta E)}{d(\Delta E)}\Big[\Delta E \le E_B\Big] = \frac{d\sigma(\Delta E)}{d(\Delta E)}\Big[\Delta E = E_B\Big] \qquad (43)$$

For Al, Valkealahti and Nieminen (1983) used a binding energy of 84 eV for the 8 L-shell electrons and a binding energy of 6 eV for the 3 valence electrons.

3.4. Extensions to non-free electron solids

3.4.1 Nearly-free electron solids. Even in a normal metal the valence band electrons are only quasi-free and are better described as Bloch functions. To evaluate the transition probability between Bloch states $|k,n>$ with energy $E_{k,n}$, Rösler and Brauer (1981a,b; 1988) used the Fermi golden rule:

$$W(\vec{k}_p\, \nu_p, \vec{k}'\nu' \,|\, \vec{k}'_p\, \nu'_p, \vec{k}\nu) = \frac{2\pi}{\hbar} \sum_q \frac{V_q^2}{|\varepsilon(\vec{q}, E_{\vec{k}_p \nu_p} - E_{\vec{k}'_p \nu'_p}|^2}$$
$$|<\vec{k}'_p\, \nu'_p \,|\, \exp(i\vec{q}\vec{r}) \,|\, \vec{k}_p\, \nu_p>|^2 |<\vec{k}\, \nu \,|\, \exp(-i\vec{q}\vec{r}) \,|\, \vec{k}'\nu'>|^2$$
$$\delta\left(E_{\vec{k}'_p\, \nu'_p} + E_{\vec{k}\, \nu} - E_{\vec{k}_p\, \nu_p} - E_{\vec{k}'\nu}\right) \qquad (44)$$

Then, they derived from this transition probability, the excitation function $S(\vec{k}_p,\vec{k})$ they had to incorporate into the Boltzmann transport equation. The excitation function $S(\vec{k}_p,\vec{k})$ expressed the number of metal electrons promoted by the primary beam into the state $\vec{k}$, per unit primary current and unit volume. It could be deduced from W by the relation:

$$S(\vec{k}_p, \vec{k}) = \frac{m}{\hbar k_p} W(\vec{k}_p, \vec{k}) \qquad (45)$$

$S(\vec{k}_p,\vec{k})$ was taken as the sum of the three contributions associated with the individual excitations from the band valence (ind), the bulk decay plasmon (bp) and the ionic core ionization (c) :

$$S(Ep, \vec{k}) = S_{ind}(Ep, \vec{k}) + S_{bp}(Ep, \vec{k}) + S_{core}(Ep, \vec{k}) \qquad (46)$$

An usual technique in resolution of the Boltzmann transport equation is to handle the angular dependence of the problem by expansion into Legendre polynomials. Therefore, there is a simple relation between the mean free path associated with an excitation process and the corresponding zero-order term $S_0(E, E')$ of the Legendre polynomial expansion. For instance, for the individual collisions, one has:

$$\lambda_{ind}^{-1}(E) = 4\pi \int_{E_F} dE'\, S_{ind}^{(0)}(E, E') \qquad (47)$$

From a comparison with the Streitwolf excitation function, one can write:

$$S_C(E, E') = S_{ind}^{(0)}(E, E') \qquad (48)$$

To simplify their calculations, Rösler and Brauer considered that the conduction electrons could be partially described as forming a free-electron-gas. For instance, for screening (see the expression of W), they used the RPA dielectric function, as given by the Lindhard expression. They considered also different other approximations for the dielectric function as $\varepsilon(q,\omega)=1$ (Streitwolf) or $\varepsilon(q,\omega)=1+k_{TF}^2/q^2$ (Thomas-Fermi approximation). Calculations including the full Lindhard expression for the dielectric expression showed that dynamical screening is of great importance. Comparison of results illustrated that the excitation rate was overestimated by Streitwolf and greatly underestimated by the Thomas-Fermi approximation (see Fig. 6).

The plasmon linewidth $\Gamma(q)$ was calculated from a dielectric matrix in which the matrix elements were evaluated from squares of Bloch integrals. The Bloch integral is defined by :

$$B^{\vec{G}}(\vec{k}, \vec{k}') = \frac{1}{\Omega_0} \int_{\Omega_0} u_{\vec{k}}^*(\vec{r})\, u_{\vec{k}}'(\vec{r}) \exp\left(i\vec{G}\,\vec{r}\right) d^3\vec{r} \qquad (49)$$

where $u_{\vec{k}}(r)$ is the periodical part of the Bloch function. Its square is calculated in a perturbation theory with respect to a model potential. Different model potentials were considered (non local and local Heine Abarenkov Animalu model potential (see Heine (1970)), Ashcroft model potential (see Ashcroft (1966)) and the results for plasmon damping were calculated. Only the interband contribution to the plasmon decay was taken into account in the Rösler and Brauer calculations. In such a case, the results obtained for $\Gamma(q)$ from the Ashcroft model potential describe satisfactorily the experimental results by Raether (1965). The results deduced from the Ashcroft model potential for the zero-order term $S_{bp}^{(o)}(E,E')$ of the excitation function by plasmon damping are ex-

hibited in Fig. 7 where they are compared with similar results for the excitation function by electron-electron scattering and by inner-shell ionization.

The excitation of core electrons was described in the OPW formalism by Rösler and Brauer and the results were compared with those obtained from the Gryzinski model or by Tung and Ritchie (1977) from the atomic generalized oscillator strengths calculated by Manson (1972). In comparison with the OPW formalism, the Gryzinski model gave a larger number of excited electrons at low energies and a smaller number at high energies, than in the OPW formalism. The results obtained from the generalized oscillator strengths appeared as intermediate between those of Gryzinski and those obtained in the OPW model (see Fig.7).

3.4.2 Use of the optical loss function. The earliest work on the connection between secondary electron emission and optical conductibility was performed by Baroody (1956) in the assumption of an unscreened interaction between conduction electrons and primary electrons. This connection was extended to screened interaction between outer-shell electrons and energetic electrons by Cailler (1969) in the scheme of the Boltzmann transport equation. The electron transition probability was deduced from optical measurements and the possibility of the presence of structures in the secondary electron peak of noble metals was then theoretically predicted. Many studies of the secondary electron emission of noble metals were made by the Nantes team (see Cailler and Ganachaud (1972) Ganachaud and Cailler (1973 a,b)) Mignot (1974), Dejardin-Horgues *et al.* (1976), Ganachaud (1977) and Pillon *et al.* (1977)). Though a general description of the secondary electron emission properties of noble metals could be given, it was however concluded from these studies that a refined description of the elastic and inner-shell ionization processes was required to improve agreement between simulated and experimental results.

A particular requirement in the study of the response function of rather highly localized states, is to take into account the existence of a local field different from the mean macroscopic field, because of the polarization of these states (see Nagel and Witten (1975)). The effects of this local field on the dielectric function have been considered by several authors (see for instance, Cailler *et al.* 1983). Ritchie and Howie (1977) have analyzed the requirements coming from the sum rules for the extension of the "optical" dielectric function to non-zero values of q. Using a procedure similar to

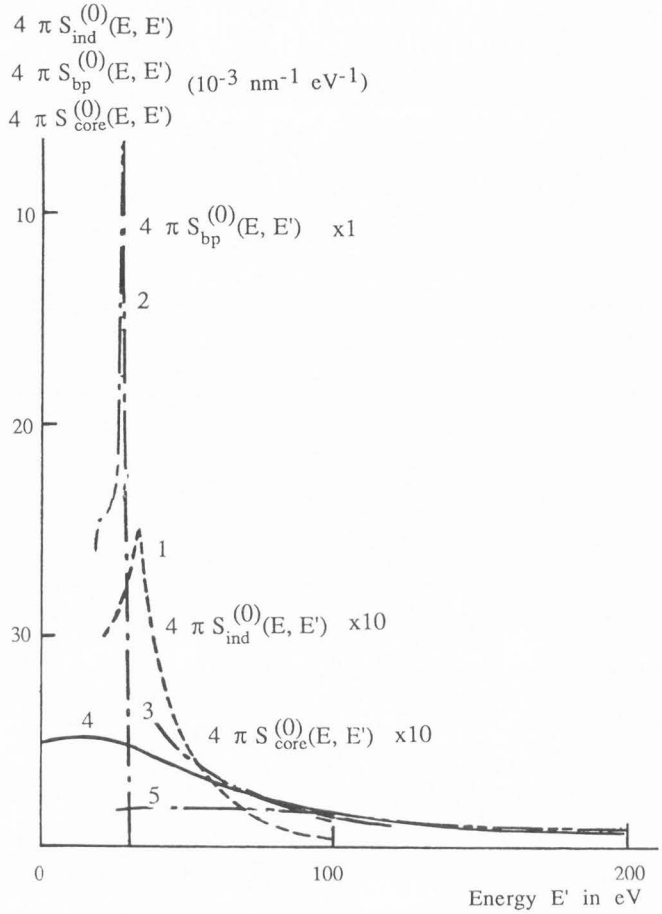

Fig.7 : Energy dependent excitation functions
- $4\pi\ S_{ind}^{(0)}(E,E')$: by electron-electron scattering in the Lindhard dynamical screening approximation (1),
- $4\pi\ S_{bp}^{(0)}(E,E')$ by plasmon damping (2) and,
- $4\pi\ S_{core}^{(0)}(E,E')$ by L inner-shell ionization Gryzinski (3) Generalized oscillator strengths (4) and Orthogonalized plane wave (5)
E' is the final energy of the excited electron and E is the initial energy of the energetic electron.The results were obtained for an energy E = 2 keV. (After Rösler and Brauer (1981b)).

that of Ritchie and Howie, Cailler *et al.* (1981) evaluated the mean free path in copper.

The use of the optical loss function for calculating the inelastic mean free path and studying the slowing down of the electrons has now become very popular. Penn (1987) proposed an algorithm in which the loss function is determined from a statistical approximation of the imaginary part of the inverse Lindhard dielectric function and from a knowledge of the optical or electron-energy loss function. This algorithm was used by Penn (1987) and Tanuma *et al.* (1988) for

calculation of inelastic mean free paths in different materials. Ding and Shimizu (1988,1989) proposed a theoretical model for Monte-Carlo simulation of backscattering and secondary electron generation by keV electrons In this model the calculation of the inelastic mean free path was based on the use of the experimental dielectric function $\varepsilon(\omega)$.

$$\frac{d\sigma_{in}(\Delta E)}{d(\Delta E)} = \frac{a_0}{2\pi}\frac{1}{N_{at}E}\,\mathrm{Im}\left\{-\frac{1}{[\varepsilon(\Delta E)]}\right\}\ln\frac{cE}{\Delta E} \qquad (50)$$

In this relation, $\Delta E = h\omega$ and c is a constant to be determined so that the calculated inelastic mean free path fits the experimental data in a wide energy range. The simulations were performed for Si, Cu and Au samples and the results which were obtained agreed well with experiment.

3.4.3. Semiconductors and insulators. The most pertinent work using dielectric response functions of model semiconductors and insulators was performed by Ritchie and co-authors. For instance, Emerson *et al.* (1973) studied the electron slowing-down spectrum in silicon, Ritchie *et al.* (1975) that of electrons in several materials including Si and Al_2O_3 and Tung and Ritchie (1977) that of electrons in Al_2O_3. A quite different approach was proposed by Penn (1976) who suggested describing the 24 valence electrons of Al_2O_3 as if they were free and by Jousset (1987a) who considered the electron emission from Al through a thin film of Al_2O_3 (see section 4).

3.5. Conclusion.

From this section, we can retain the importance of the dynamical screening for a realistic estimation of the individual collision probabilities, the need for a consideration of crystalline effects in a description of the plasmon damping and the fact that the Gryzinski cross section overestimates the low energy electron creation probability during an ionizing core event and underestimates the high energy electron creation probability. At last, it can be noticed that important developments in the case of non-free electron materials remain to be made.

4) Simulation models.

4.1. Monte-Carlo simulation methods

In principle, calculations with a Monte-Carlo simulation method require theoretical knowledge of all the cross sections associated with the various types of collisions. Whenever these requirements are fulfilled, a direct simulation is possible. However as mentioned before, for a description of the true secondary peak it is necessary to follow all the electrons of the cascade which maintain an energy above the vacuum level. Consequently, a long time of computation is needed and in fact, there are only a few number of theoretical descriptions of the secondary electron emission with simulation models. Taking into account the computer time consumption and the needed accuracy of the results, one has to estimate the necessity of using a refined description of each interaction mechanism. In other words, one has to identify the parameters which have to be described with precision and those which can receive a highly simplified description. For other studies as the electron transmission, the electron backscattering, the Auger electron escape, or still to simulate the energy loss spectrum, one may accept more easily, less elaborate but sufficiently efficient descriptions.

The Monte-Carlo method is based upon the statistical concept of a trajectory for the particles which take part in the transport process in the solid. A trajectory is a sequence of straight line paths or steps, separated by interaction "points". According to the mode of break of the trajectory between steps and the mode of description of the interactions, the different simulation models can be roughly divided into three categories :

4.1.1. The continuous slowing down approximation models. They were applied by Shimizu *et al.* (1970,1972) to investigate the energy dissipation of electrons in several targets. In these calculations, each step was taken of a given finite length. At the end of each step the direction of motion of the electrons was changed according to an elastic scattering formula (the screened Rutherford scattering cross-section, for Shimizu *et al.*) and their kinetic energy was reduced by an energy loss derived from Bethe's energy loss equation. This treatment is inappropriate to describe the energy distribution of scattered electrons. Indeed, in the model all the electrons lose continuously their energy, whilst the real energy loss processes should obey a Poisson distribution. In other words, the theoretical model does not take into account the possibility for an electron to lose in a single collision, a large fraction of its energy and in another one, to suffer only a very small energy loss. Therefore, from the simulation distribution, the highest electron energy is lower than the primary energy from a finite value, whereas in the experimental distribution, a fraction of the electrons are emitted with an energy equal to or only slightly lower than the primary energy.

4.1.2. The single scattering type models. In these models, still called "direct simulation Monte Carlo models", the electron trajectories are separated into straight line free paths, so that along each free path, the electrons are assumed undergoing only one scattering collision event. Berger *et al.* (1970) applied this technique to the calculation of the spatial distribution of the energy deposited by electrons in the atmosphere. The earlier versions of this category of models for a description of the secondary electron emission were given by Cailler and Ganachaud (1972), Ganachaud and Cailler (1973 a,b) and by Shimizu *et al.* (1975, 1976). In the single scattering model, the particle propagates for a free path along a straight line, keeping its classical parameters (energy and direction of the motion) unchanged. This behavior is modified in order to account for the interactions of the electron beam with components of the solid. In practical calculations, one admits that the effects of these interactions can be located at some points, the end points of the free paths, where the angle and energy characteristics of the particle suffer their accidents. These events determine completely the random concatenation of the rectilinear portions of the full trajectory.

With the assumption of a linear response of the solid to the excitation caused by a primary electron, each primary particle is followed individually, as well as all the electrons of the cascade which it generates. Except for particles close to the surface, the solid is considered to be a homogeneous medium. A normal metal as aluminium for instance, is usually described by a randium-jellium model. In such a model, the delocalized electrons of the jellium are regarded as an electron gas. The ionic cores are assumed to be embedded in the jellium and randomly distributed, according to a uniform background model (randium). This, of course, precludes any direct treatment of the diffraction effects.

Under these conditions, the propagation of an electron in the solid becomes a stochastic process, and one generally admits that the elastic and inelastic collisions it suffers can be described by a Poisson distribution law. An elastic collision represents a global interaction process with the potential field surrounding the ionic cores. An inelastic collision can result from various effects (individual collisions with the electrons of the jellium, collective excitations of the electron gas, ionization of the inner shells), for which the energy losses and the angular deflections follow dissimilar laws.

4.1.3. The multiple collision model. This kind of model was recently used by Werner and Heydenreich (1984) in a study of the electron transmission and backscattering. In such a model the number of scattering events to be simulated is rapidly decreased by uniting many single scattering events into one multiple scattering event. For that, Werner and Heydenreich used a model in which the multiple scattering is approximated by a modification of the screening factor β in the screened Rutherford scattering cross-section. Therefore, only one parameter was to be determined in order to attain the correct atomic number and energy dependence. In the screened Rutherford scattering description, the relative scattering probability per solid angle element is written :

$$\frac{d\sigma_{el}}{d\Omega} \Big/ \left(\int_{\Omega_{tot}} d\Omega \frac{d\sigma_{el}}{d\Omega} \right) = \frac{\beta\,(1+\beta)}{\pi} \frac{1}{(1+2\beta-\cos\theta)^2} \qquad (51)$$

Werner and Heydenreich remarked that the above angular distribution included precisely two distributions which are formed by the scattering process :

- the single scattering distribution given by $\beta = \beta_0$.
- the isotropic distribution resulting from an infinite number of scattering events (given by $\beta=\infty$).

Between these two limiting cases, they have considered that the spreading by multiple scattering of the incident electron beam could be described by an appropriate value of the generalized screening number β. β had to be a monotonously increasing function of the mean number of elastic scattering events w and was written under the form :

$$\beta = \beta_0 \; w^n \qquad (52)$$

where β_0 is the value of the screening parameter in case of single scattering. They used for the single scattering screening parameter, the following expression :

$$\beta_0 = c_1 \frac{Z^{2/3}}{E} \quad \text{with } c_1=4.34 \text{ eV.} \qquad (53)$$

An equivalent form of this consists in replacing the corrected Thomas-Fermi radius ρ_s by:

$$\rho_s^* = \frac{\rho_s}{w^{n/2}} \qquad (54)$$

The constant n was determined by calculating the backscattering probability with a Monte Carlo

simulation of w single scattering events, and was found as being nearly equal to 1.3. Hence, the generalized screening parameter is: $\beta = \beta_0\ w^{1.30}$ where β_0 is the value of the screening parameter in case of single scattering. Therefore, Werner and Heydenreich developed their multiple scattering Monte Carlo model under the following form. The Bethe range s_0 ($s_0 = s\ (E = 0)$) where :

$$s = \frac{E_0^{5/3} - E^{5/3}}{(5/3)\ 24.6\ (\rho/A)\ Z^{4/5}} \qquad (55)$$

s in μm, E in keV, and ρ in $g.cm^{-3}$

was subdivided into m segments of the length $\Delta s_i = \Delta s$ = Const. An electron moving along the ith segment kept a constant energy E_i derived from its initial energy, the length of the path it has travelled through the solid up to reaching the ith segment and the Bethe stopping power law. The mean number of elastic interaction events that it suffered along this segment was $w_i = \Delta s/\lambda_i$ where λ_i is its elastic mean free path. The generalized screening parameter β_i is then derived from $\beta_i = \beta_0\ w_i^n$. At the end of the ith segment the electron is scattered and its scattering angle is taken from the relation :

$$\cos\theta_i = 1 - \frac{2\ \beta_i\ R}{1 + \beta_i - R} \qquad (56)$$

where R is a random number. In order to obtain a more detailed description of the scattering near the target surface, the first segment was subdivided into l segments.

A comparison between the results obtained with this simulation model and the experimental ones were considered as good.

4.2. The layer-by-layer model

This model has been developed by Jousset and co-authors (cf. Jousset (1987a,b,c and d), Dubot *et al.* (1988)) and the obtained results compared with those from the Monte-Carlo simulation methods. In the layer-by-layer model, the solid is divided in layers of small thichness Δz. For an internal electron source, for instance Auger electrons, the simulation of the escape of these electrons is started from a maximum depth z_{max}. By neglecting the elastic or inelastic deflections and the probability of multiple scattering inside a layer i, the electron distribution $j_{i-1}(E,\theta)$ in the upper layer i-1 is given by :

$$j_{i-1}(E,\theta) = S_{i-1}(z)\ \Delta z\ f(E,\theta) + \exp\left[-\frac{\Delta z}{\lambda_{in}(E)\cos\theta}\right] j_i(E,\theta) + \int_E^{E_c} dE' \left\{1 - \exp\left[-\frac{\Delta z}{\lambda_{in}(E)\cos\theta}\right]\right\} j_i(E',\cos\theta)\lambda_{in}(E')\ \frac{dp(E',E'-E)}{dE'} \qquad (57)$$

On the right hand side, the first term represents the energy and angular distribution of the electrons which are generated in the layer i-1. The creation rate per unit depth S(z) is assumed constant and f(E,θ) is the normalized energy and angular distribution of the created electrons. The second term describes the number of electrons which had an energy E on the boundary between the layers i and i-1 and which do not undergo an inelastic collision in the layer i-1. In this term, $\lambda_{in}(E)$ is the total inelastic mean free path of an electron of energy E. The third term represents the number of electrons which had an energy ranging from E to E_c when they are crossing the boundary between the layers i and i-1 and which acquire an energy E in the layer i-1, as a result of an inelastic collision. In such a case, the electrons are followed until they leave the material or loose too much energy.

If the elastic or inelastic deflections are not neglected, additional terms have to be included in the above equation. As a consequence, a forward and a backward beam are generated in every layer. Therefore, a satisfactory solution of the problem can only be reached if all these scattered beams are taken into account, that is after several runs. For instance, for an internal source the z-range is covered in a first run layer-by-layer from z_{max} to the surface and the complete equation including the scattering effects and the source function S(z) is solved layer after layer. The forward beam created in the layer i is therefore included in the equation of the upper layer i-1, as it was made in the case where the deflections were neglected. The backward beam is memorized in order to be taken as internal source function $S_i(z)$ in a second run. In this second run the z-range is covered from z = 0 to z = z_{max} and again the transport equation is solved layer after layer. Generally, several subsequent runs going alternatively from z_{max} to the surface and from the surface to z_{max} are required to reach a sufficiently convergent solution (see section 5). However, if we are only interested by the energy loss spectrum near an elastic peak, the layer-by-layer method is rapidly convergent and a very

small number of runs are needed. Sometimes only one run is sufficient. In such a case, the method is particularly efficient.

4.3. The Boltzmann transport equation

Earlier work on this topic was performed by Wolff (1954), Stolz (1959), Streitwolf (1959), Hachenberg and Brauer (1959), Puff (1964), Amelio (1970), Bennett and Roth (1972), Moulin *et al.* (1973) and Sickafus (1977 a,b). This topic was largely studied by Schou (1980 a,b) and by the Nice (see Bindi *et al.* (1980), Lanteri *et al.* (1980, 1981, 1982, 1986)) and Brussels (see Devooght *et al.* (1987), Dubus (1987) and Dubus *et al.* (1987)) teams. Methods they used and results they obtained were recently exposed in SEM (Bindi *et al.* (1987), Lanteri *et al.* (1988), Schou (1988)) and will be not considered here.

5) Results obtained from simulation models.

5.1. Earlier results.

Many results obtained with simulation models can be found in the papers by Shimizu and co-authors or by Cailler and co-authors. However, only few papers are related with secondary electron emission which were published. Sources of such results can be found for instance in Ganachaud's thesis (1977) and Mignot's thesis (1974) Some results on the angular distribution from Al were included in part I. We can illustrate this section with some results on the yield curves and the energy distributions. (see Figs. 8-11).

Among the more recent results, we can mention the following ones.

Shimizu and Ichimura (1981a,b) studied by simulation the quantitative correction of electron backscattering effects in quantitative Auger analysis. They also studied by simulation the backscattered primary electron spectra n(E) above 100 eV, for Al (see Shimizu and Ichimura (1983)) . For that, they utilized the differential elastic cross-sections obtained by PWA, a Gryzinski's excitation function for inner-shell excitation, a Streitwolf's excitation function for the individual conduction electron excitations, a Quinn's mean free path for plasmon excitation. The calculations were done for primary energies of 1.5 and 3 keV and for incidence angles of 0 and 45°. The results showed a satisfactory agreement with experimental distributions. This indicated that the direct Monte-Carlo methods could be very useful for understanding penetration and backscattering mechanisms. With the same model and in the same conditions for the primary electrons,

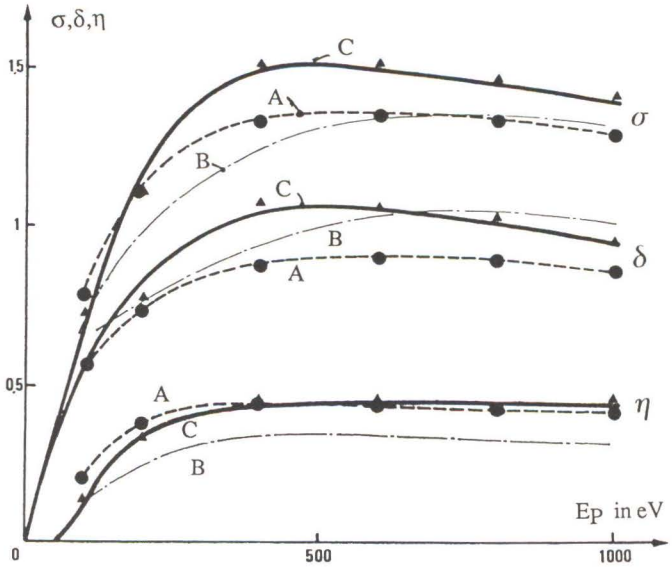

Fig. 8 : Cu : Primary electron energy dependence of the yields.
Experimental results, A : Goto et al. (1975), B : Pillon et al. (1976),
Simulation results, C : Ganachaud (1977).

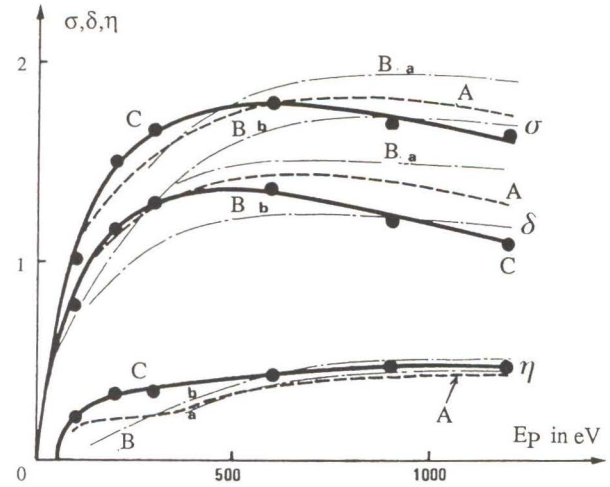

Fig.9 : Au : Primary electron energy dependence of the yields.
Experimental results, A : Thomas and Pattinson (1970), B : Pillon et al. (1976), a) after annealing, b) before annealing.
Simulation results, C : Ganachaud (1977).

Shimizu and Ichimura (1984) studied the angular distributions of backscattered and high energy secondary electrons, as well as the energy distributions for different emission angles.

Werner and Heydenreich (1984) have described the backscattering probability of primary electrons impinging in normal incidence on a solid

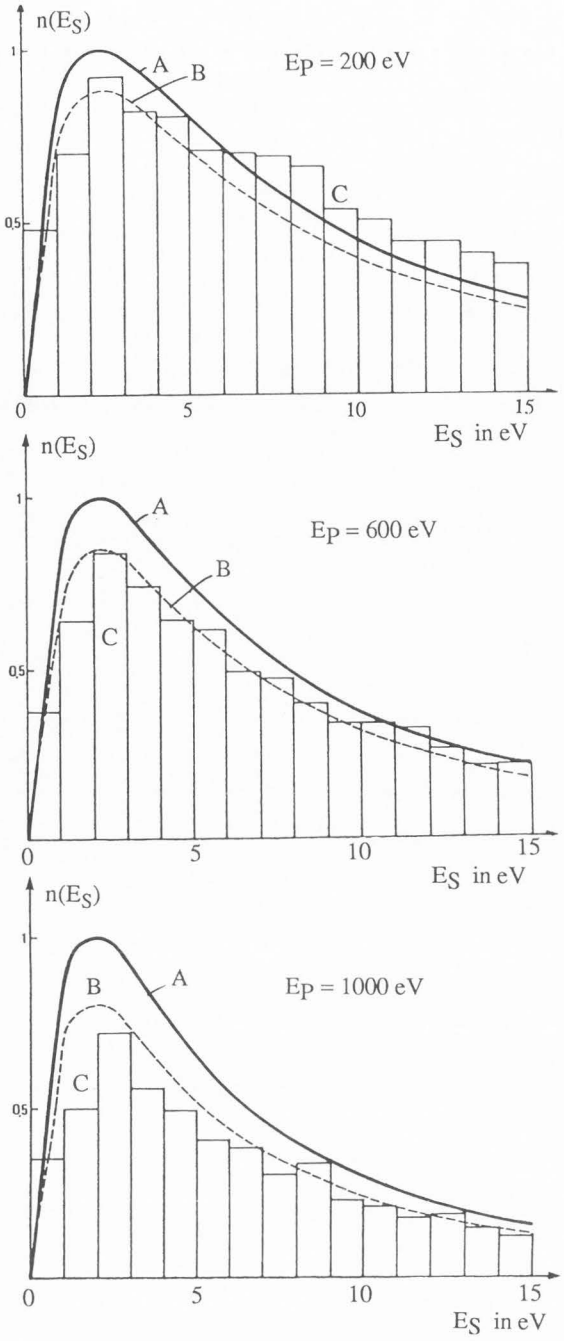

Fig.10 : Cu : Energy distribution of the true secondary electrons.
Experimental results : Both curves are from Pillon et al. (1976). They were plotted so that the area below these curves were equal to the δ values measured by Pillon et al. (1976) : curve A, or by Goto et al. (1975) : curve B.
Simulation results, curve C. (From Ganachaud (1977)).

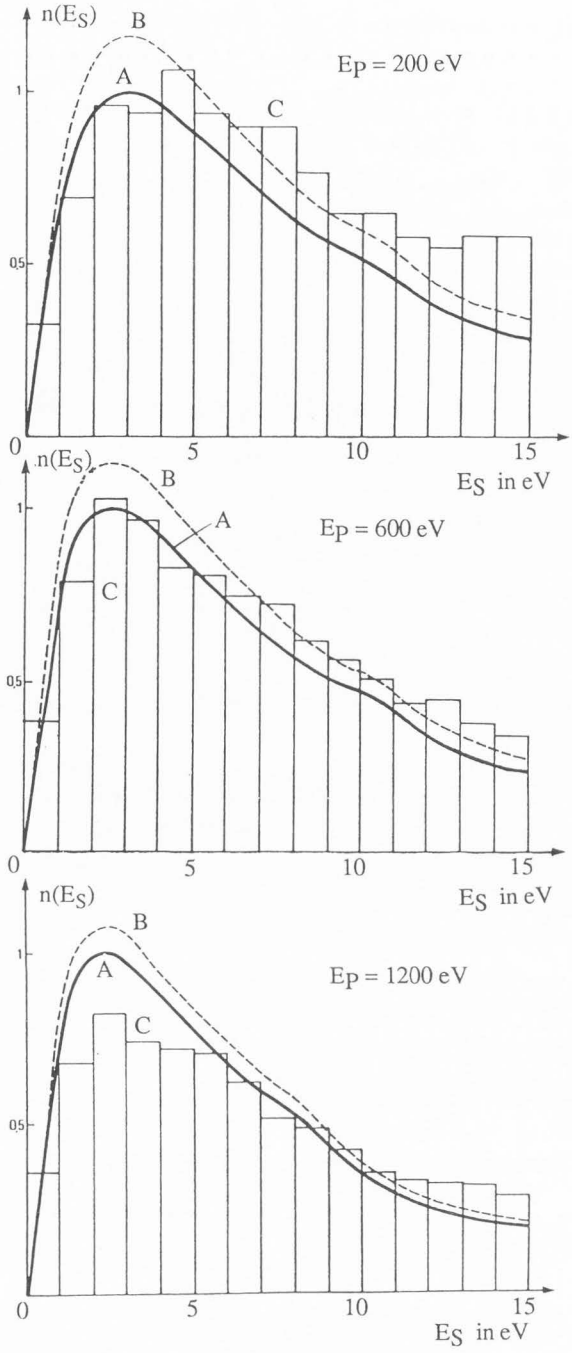

Fig.11 : Au : Energy distribution of the true secondary electrons.
Experimental results, Both curves are from Pillon et al. (1976). They were plotted so that the area below these curves were equal to the δ values measured by Pillon et al. (1976) : curve A, or by Thomas and Pattinson (1970) : curve B. Simulation results, curve C. (From Ganachaud (1977)).

target (Au, Cu, Al, C) with a primary energy of 20 keV. Their results could be satisfactorily compared with experimental results. They also studied the target thickness dependence of the backscattering probability and the energy distributions of electrons backscattered from solid Al, Cu and Au targets.

Jablonski (1985) used the first Born approximation and the Thomas-Fermi-Dirac potential as given by Bonham and Strand to study the elastic backscattering of electrons from surfaces. A direct Monte Carlo simulation model was utilized. Because Jablonski was only studying the elastic primary electron backscattering, in his simulation model, the trajectories were only determined by the elastic scattering events. The inelastic processes associated with the ith electron trajectory were taken into account according to formula

$$\Delta I_i = \exp(-s_i/\lambda) \text{ if } s_i \leq s_{max} \quad \text{and}$$

$$\Delta I_i = 0 \text{ else.} \tag{58}$$

In these relations, s_i is the path length of the ith electron trajectory. The elastic reflection coefficient was calculated as the mean value of the ΔI_i contributions. In order to determine the validity of his Monte Carlo model, Jablonski calculated the primary electron energy dependence of the elastic reflection coefficient. The calculations were performed for Al, Cu and Ag and two inelastic mfp were used, one given by Ashley and Tung (1982) and the other by Penn (1976). The experimental and the calculated values of η_E were found in reasonable agreement at energies exceeding 2 keV. For Al, the inelastic mfp is well known and the calculated result is nearly the same in both approximations. For Cu and Ag, a better agreement between the experimental result and the calculated one is observed when using Penn's mfp. At lower energies, there are divergences, and the differences seem to increase with increasing atomic number. The observed deviation can be due to the fact that the first Born approximation becomes less valid at low energies and for high atomic number elements. Another source of deviations at low energies may be the use of the Bonham and Strand potential which is adapted to the interactions between an electron and an isolated single neutral atom. However, with exception of silver, the shape of the experimental and calculated energy dependences of η_E were nearly similar in the whole considered energy range.

The Monte Carlo method was used to calculate the angular distribution of elastically backscattered electrons. The results were compared with the distribution calculated in a so-called "single scattering model" and with the cosine distribution. In the single elastic scattering model, the elastic backscattering coefficient is given by :

$$\eta_E = \sigma_{eff} N_{at} \lambda_{in} \text{ where } \sigma_{eff} = \int_{\pi/2}^{\pi} \frac{d\sigma_{el}}{d\theta} \frac{1}{1-\sec\theta} d\theta \tag{59}$$

where $d\sigma_{el}/d\theta$ is the elastic differential scattering cross-section. From this comparison, it was concluded that for carbon the majority of the backscattered electrons had undergone only one elastic collision, whereas for silver, the angular distribution was close to the cosine distribution.

Another comparison was made between the results obtained with both models, for different values of an hypothetic inelastic mean free path. It was shown that the elastic backscattering coefficient could be written under the form :

$$\eta_E = N_{at} \sigma_{eff} \lambda_{in} + D \lambda_{in}^2 \tag{60}$$

D could be obtained as a result from the Monte Carlo simulation. According to Jablonski, this result offers a convenient method for determining the inelastic mfp from experimental values of η_E. He calculated the values of the inelastic mfp, from published values of η_E and found that they were in reasonable agreement with the experimental values found in the literature.

Tholomier *et al.* (1987) used the screened Rutherford cross section in the Lenz's approximation of the screening radius: $\rho_s = a_0 Z^{-1/3}$ and the Bethe stopping power to simulate the influence of the backscattered electrons on the Auger emission from Si, Ag and Au. They showed (see Figs. 12 and 13) that for a point incident beam, the spatial distribution of the backscattered and the Auger electrons were more strongly peaked for heavier elements than for the lighter ones and at lower energy (5 keV) than at the higher ones (50 keV). However, by taking into account a finite beam spot size, Tholomier *et al.* (1988) showed that the atomic number dependence of the Auger electron spatial distribution does not influence highly the resolving power of the Auger spectrometer, which is then principally limited by the beam size.

To simulate the scattering of keV-electrons in Si, Au, SiO_2 and PMMA, Fitting and Reinhardt (1985) used a PWM-fitted screened Rutherford

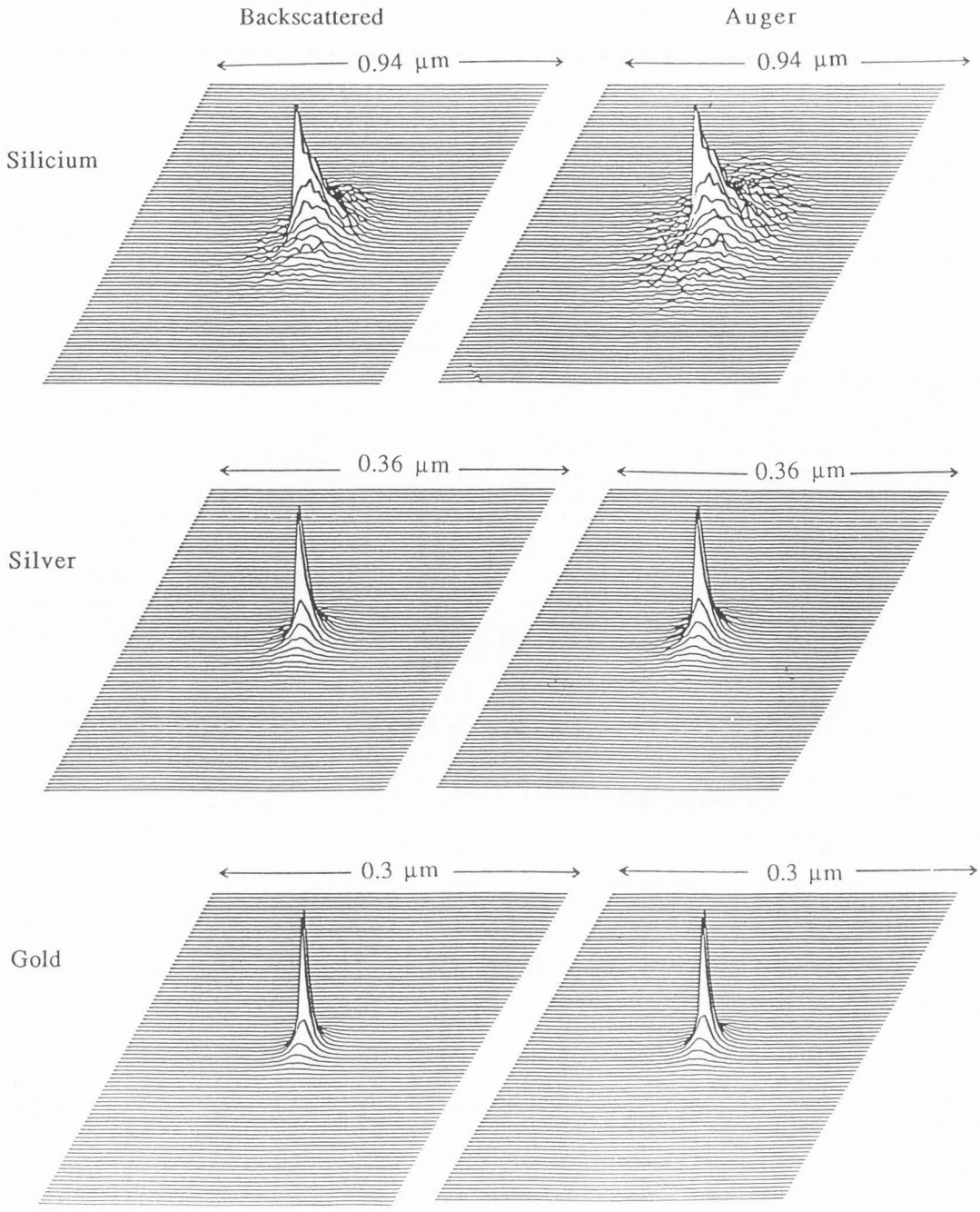

Fig.12 : Spatial distributions of the backscattered and the Auger electrons created by the backscattered electrons in Si (KL_3L_3 Auger line), Ag ($M_5N_{4,5}L_{4,5}$ Auger line) and Au ($N_7O_{4,5}O_{4,5}$ Auger line). The energy of the primary beam was of 5 keV and the incidence angle of 45°. (From Tholomier et al. (1987a)

scattering and an effective mean free path of core ionization expressed by :

$$\lambda_i = - \Delta E_i / S_{core} \approx - I_i \, / \, S_{core} \qquad (61)$$

where I_i is the ionization energy of a given core level and S_{core} the ionization stopping power. The polar angular scattering of the inelastic interaction with a core electron was approximated by a free

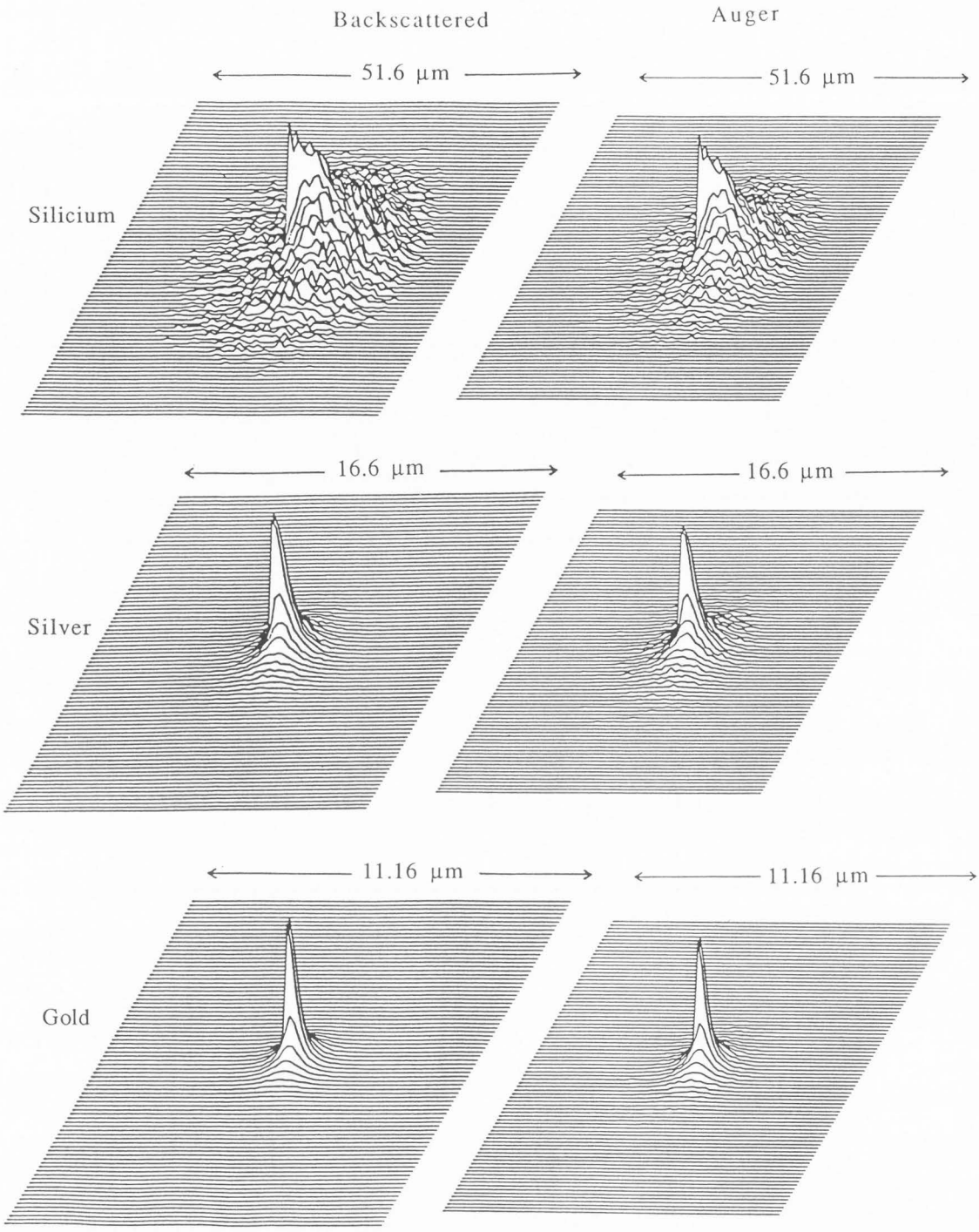

Fig.13 : Spatial distributions of the backscattered and the Auger electrons created by the backscattered electrons in Si (KL_3L_3 Auger line), Ag ($M_5N_{4,5}L_{4,5}$ Auger line) and Au ($N_7O_{4,5}O_{4,5}$ Auger line). The energy of the primary beam was of 50 keV and the incidence angle of 45°. (From Tholomier et al. (1987a)

collision momentum transfer :

$$\sin^2\theta = \Delta E_j/E \approx I_j/E \qquad (62)$$

and the ionization stopping power was estimated from data given in the literature. The interaction of electrons with valence band electrons, and the

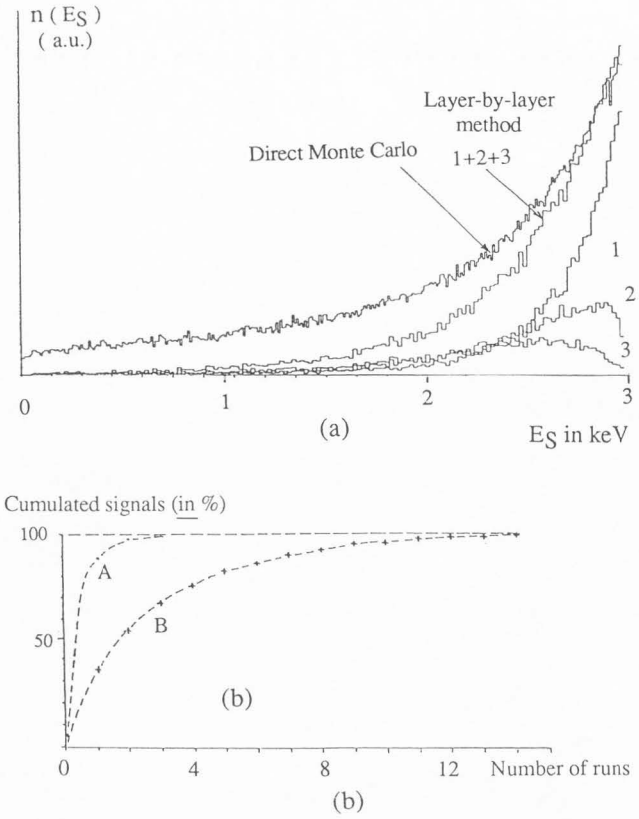

Fig.14 : Comparisons between the theoretical results obtained with the layer-by-layer method according to the number of runs (1, 2 or 3) and with a direct Monte Carlo simulation method. The target was in Cu and the primary energy was 3000 eV. (a) Energy distributions, (b) Cumulated signals evaluated with the help of the layer-by-layer model, in % of the corresponding direct Monte Carlo results. (A) : electrons emitted with an energy ranging from 2900 to 3000 eV, (B) electrons emitted with an energy lower than 2900 eV (From Jousset (1987a)).

collective interaction with plasmons were described by the dielectric energy loss function :

$$\frac{\partial^2\sigma_D}{\partial(\Delta E)\partial\Omega} \sim \frac{1}{q^2}\,\mathrm{Im}\left(-\frac{1}{\varepsilon}\right) = \frac{1}{q^2}\,\frac{\varepsilon_2}{\varepsilon_1^2+\varepsilon_2^2} \qquad (63)$$

with :

$$q^2 = K^2 + K'^2 - 2KK'\cos\theta \qquad (64)$$

and,

$$\frac{\hbar^2 K'^2}{2\,m} = E' = E - \Delta E \qquad (65)$$

The polar scattering probability of the electron was obtained by substituting q^2 value in the dielectric energy loss function. The mfp λ_D for a dielectric loss was evaluated by :

$$\frac{1}{\lambda_D} = \frac{1}{\lambda_{exp}} - \frac{1}{\lambda_{core}} \qquad (66)$$

and the dielectric losses ΔE were obtained by integration of the loss function and with the help of a random number R :

$$\frac{\int_0^{\Delta E} dE\ \mathrm{Im}(-1/\varepsilon)}{\int_0^{100\ \mathrm{eV}} dE\ \mathrm{Im}(-1/\varepsilon)} = R \qquad (67)$$

The angular, energy and depth distribution of the backscattered electrons were obtained in dependence on the angle of incidence, for Si, Au, SiO_2 and PMMA targets.

Jousset (1987a), Jousset *et al.* (1987 b,c,d) presented detailed results in the case of a target of Cu or of Al covered with a thin layer of alumina. They proceeded to simulations with either the direct simulation method or the layer-by-layer method. In the case of the Cu target, comparisons between the theoretical results obtained either with the layer-by-layer method or the direct Monte Carlo simulation technique were performed (see Fig.14). They showed that near the elastic peak the results obtained after a few number of runs in the layer-by-layer method were quite comparable to those obtained with the Monte Carlo simulation technique. In this case, the layer-by-layer method is rapidly convergent and therefore it appears very interesting if energy loss spectra have to be described. On the contrary, far from the elastic peak, the layer-by-layer method is only slowly convergent and consequently it does not bring any amelioration as compared with the direct simulation technique.

The emissive properties of an Al target covered with a thin film of alumina were studied by Jousset (1987a). In the case of simulation by a direct Monte Carlo model, the Al substrate was described in the randium-jellium model. The assumptions which were made followed the main lines of the Ganachaud and Cailler model. For Al_2O_3, a mean valence binding energy of 14 eV was assumed and the jellium cross-section was calculated by a Gryzinski approach. In the layer-by-layer model, the creation of the secondary electrons was assumed isotropic and a value of 250 Å was chosen for z_{max}. The energy distribution and relaxation probabilities of the KLL Auger electrons were obtained from theoretical calculations. The

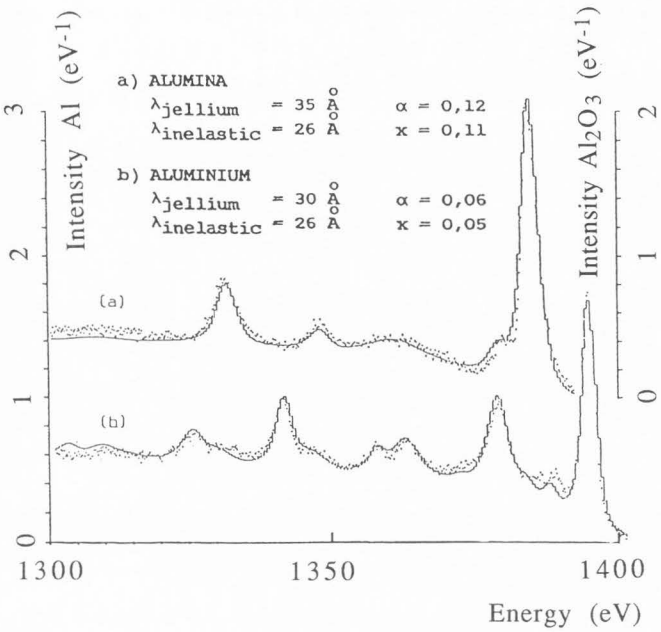

Fig.15 : KLL Auger spectra from a target made of Al and covered with a thin alumina layer. Comparisons between the experimental spectra (·····) and the theoretical results (———) obtained with the layer-by-layer method. (From Jousset (1987a)). α is the asymmetry parameter of Doniach and Sunjic (1970), x is the probability of intrinsic plasmon creation and for the inverse mean free paths :

$$\lambda_{jellium}^{-1} = \lambda_{ind}^{-1} + \lambda_{bp}^{-1} \quad \text{and} \quad \lambda_{inelastic}^{-1} = \lambda_{jellium}^{-1} + \lambda_{core}^{-1}$$

widths of peaks were adjusted to experiments and intrinsic individual processes were included as a Doniach-Sunjic shape for the peaks (see Doniach and Sunjic (1970)), with an asymmetry parameter α. The probability x of intrinsic plasmon creation were introduced in the excitation function S(E). For Al_2O_3,the intensities of the Auger peaks were taken identical to those in Al, but the energies were shifted by about 9 eV to lower values of the energy. Calculated spectra were convoluted by a Gaussian function to account for the analyser resolution (in the range 1-2eV).

Experiments were carried out on Al samples issued from high purity polycristalline wafers and covered with Al_2O_3 thin film obtained by an anodic oxydation in tartric acid bath. Experimental spectra were recorded with a MAC 2 analyser from Riber. They were compared to simulation results after subtraction of a background which was fitted in the high energy region with an exponential law and then extrapolated below the Auger peaks.The layer-by-layer calculation and the direct Monte Carlo simulation were shown to be in

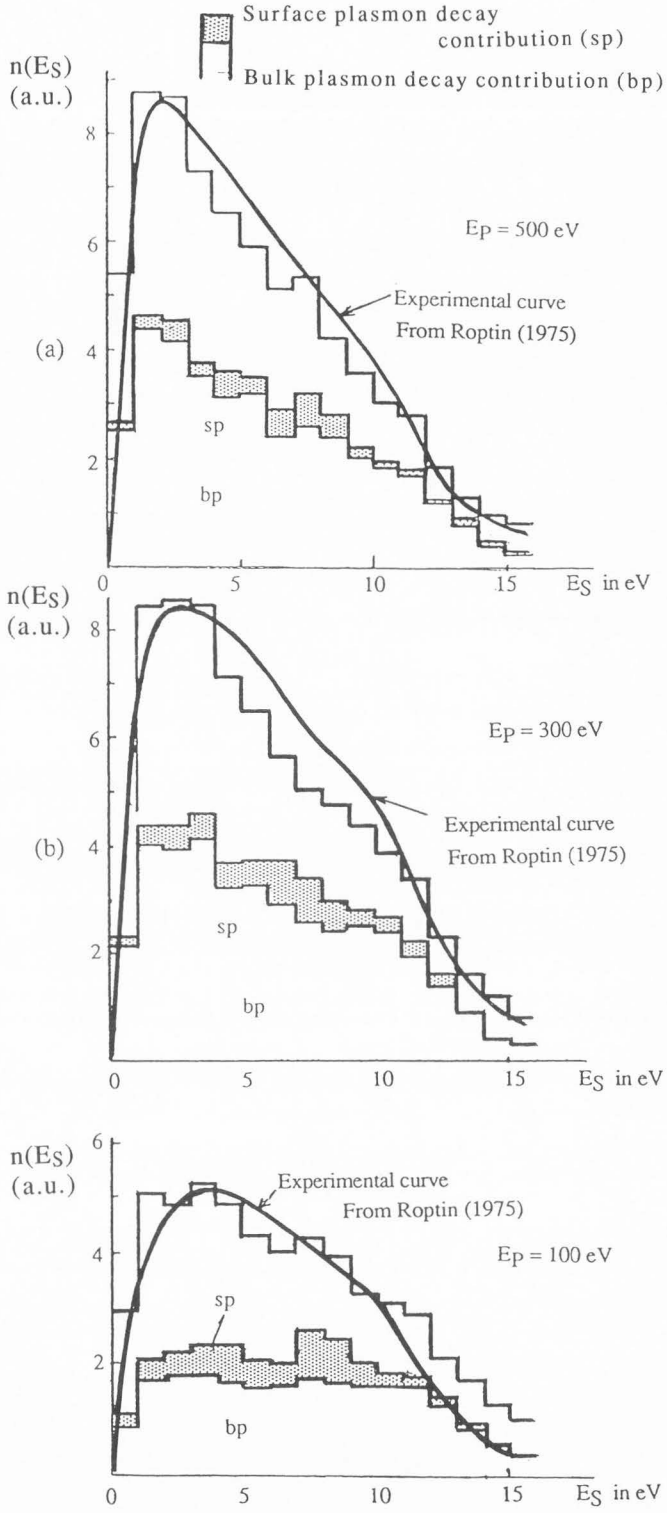

Fig.16: Contribution of the bulk- and the surface-plasmon decays to the true secondary peak from Al.

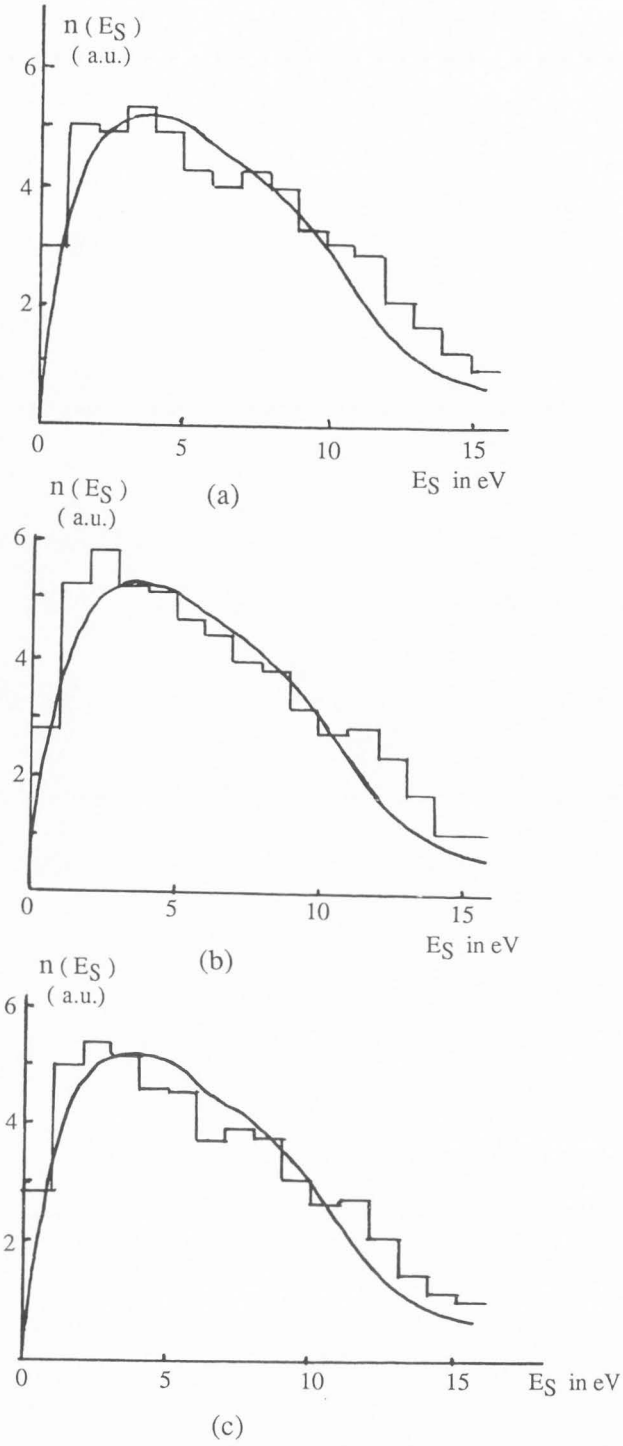

Fig.17: True secondary electron peak. Influence of the plasmon decay mode.
a) $p_{b1}=1$; $p_{b2}=0$; $p_{s1}=1$; $p_{s2}=0$,
b) $p_{b1}=0.75$; $p_{b2}=0.25$; $p_{s1}=1$; $p_{s2}=0$.
c) $p_{b1}=0.75$; $p_{b2}=0.25$; $p_{s1}=0.75$; $p_{s2}=0.25$.

complete concordance when no deflection was accounted for and when a limited size was given to the model layers (Δz= 2Å).

The elastic (described with a screened Rutherford model) and inelastic (assuming the free electron law : $\sin^2 \Delta\theta = \Delta E/E$) deflections affected only weakly the spectrum in the KLL Auger energy range (1250-1400 eV). The agreement between the layer-by-layer calculations and the experimental spectra was good (see Fig.15), indicating that the values deduced from the randium-jellium model were realistic.

Dubot *et al.* (1988) presented for the LMM Auger spectra from copper, a comparison between experimental and simulated results. They used the direct simulation and the layer-by-layer models. The results obtained with the help of the layer-by-layer method showed numerically that the influence of inelastic and elastic deflection was negligible in the near peak domain. Furthermore, they reproduced fairly well the LMM Auger spectrum from Cu.

Kotera (1990) described secondary electron emission from Cu. For that, he used a calculation model which was the same as proposed by Koshikawa and Shimizu (1974).

5.2. Critical analysis of a Monte-Carlo model.

We shall first consider some results we have recently obtained for the true secondary peak from Al. We present calculations made for three primary energies E_p=100, 300 and 500 eV. They will be compared to the measurements performed by Roptin (1975) some years ago with a 4-grid analyser (see also Pillon *et al.* (1976). The energy distributions are shown in Figs.16 a,b and c. We have shown on each histogram the part of the true secondary electron distribution that is due to the volume plasmon decay and the part that is due to the surface plasmon decay. We have assumed that each of these effects leads to the creation of one electron-hole pair.

We see that the volume plasmon damping contributes for a very important part (up to 50%) to the intensity of the secondary peak. The contribution of the surface plasmon damping is much more moderate (less than 10%). We have assumed that the plasmon energy $\hbar\omega_p$ was transferred to an electron of initial energy E' in the Fermi sea according to the law $\rho(E')\ \rho(E'+\hbar\omega_p)$ where $\rho(E)$ represents the density of states in the valence band. For the sake of simplicity, we have neglected any wave-vector conservation and the probability of transfer was simply taken proportional to the product of the densities of the occupied states of

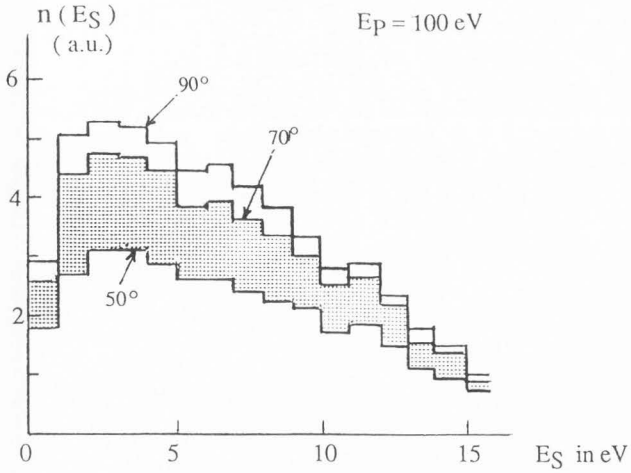

Fig.18 : True secondary electron peak from Al. Influence of the maximum collection angle.

energy E' and the empty states of energy E'+ħω. For aluminium, we have taken ρ(E) as being proportional to $E^{1/2}$. Thus, the plasmon damping contributions have a rather large extension in energy. Furthermore, the dispersion relation, as predicted by the dielectric theory gives itself a substantial width to the plasmon loss peak. So, the "fine structure effects" which appear as rather well localised shoulders in the true secondary peak are only roughly accounted for by our model.

We can observe that the volume plasmon contribution varies in shape with the primary energy E_p. As E_p increases, the electrons which are due to the volume plasmon damping are created deeper in the solid. The collisions they suffer before reaching the surface reinforce the low energy part of the bulk plasmon damping contribution. For a better presentation of the results in Fig.16 we have, for one energy (here E_p=500eV), adjusted the heights of the experimental and theoretical (Fig.16a). We shall come back to this point in what follows. The overall agreement for the shape of the true secondary peak (position of its maximum and its half-height width) is satisfactory in the whole.

For a primary energy of 100 eV, we have presented in figs.17a,b and c, the evolution of the true secondary peak when one assumes that the volume (or surface) collective excitation can decay by creating one electron-hole pair with a probability p_{b1} (or p_{s1}) or by two electron-hole pairs with a probability p_{b2} (or p_{s2}). In figs.17a,b and c the sets of values for p_{b1}, p_{b2} , p_{s1} and p_{s2} are (1,0,1,0), (0.75, 0.25,1,0) and (0.75,0.25,0.75,0.25), respectively. Both processes (one and two electron-hole pair creation) presumably take place, the first one being predominant. Thus, in what follows it will be the only process considered.

Let us now come back to the kind of adjustement that is included in our results in Fig.16. For the true secondary yield δ, we find a theoretical value of 0.75 for a primary energy of 100 eV, whereas Roptin (1975) had obtained an experimental value of 0.57. The discrepancy is presumably due for a large part to a collecter aperture effect. Indeed, in our Monte Carlo program we had, up to now, assumed that the secondary electrons emitted by the target were subsequently collected in a solid angle of 2π steradians. In the experiment performed by Roptin with its four-grid analyser, the collection angle was of 50°. So, we have made additional calculations by varying the collection angle θ_c and the corresponding results are shown in Fig.18. The theoretical values obtained for δ were of 0.44, 0.67 and 0.75 for collection angles of 50, 70 and 90°, respectively. This variation of the theoretical true yield is in complete agreement with that obtained from a cosine distribution of the secondary electrons. Indeed, in such a case, the collection angle dependence of δ will be proportional to $(1-\cos\theta_c^2)$. Multiplying 0.75 by this latter factor for θ_c = 50 and 70°, gives 0.44 and 0.66, that is almost exactly the results obtained by simulation. The same calculation, performed for θ_c = 60°, gives 0.56, very close to the experimental value. For a primary energy of 500 eV and for a collection angle of 90°, we obtained a theoretical true yield of 0.83. Multiplying this result by $(1-\cos\theta_c^2)$ for θ_c= 50° and 70° gives 0.49 and 0.73, whereas the Roptin result is of 0.66. The reason why the calculated results for θ_c= 50° are too small in comparison with experiment is not known. However, we can notice that the values of the ratio δ_{exp}/δ_{th} are nearly the same at each primary energy.

To judge the validity of a simulation model, the basic questions are to know which are the principal physical processes to introduce into the model, the precision with which they are known and the precision with which they have to be described. Obviously, for a simulation of the secondary electron emission, the important processes are the elastic collisions with the ionic cores or the inelastic collisions with the electrons of the valence band. For Al, it is quite so evident that plasmon decay has to be introduced, as it can be seen from the results of Fig.16. Less evident a priori is the influence of the ionizing collisions with the ionic

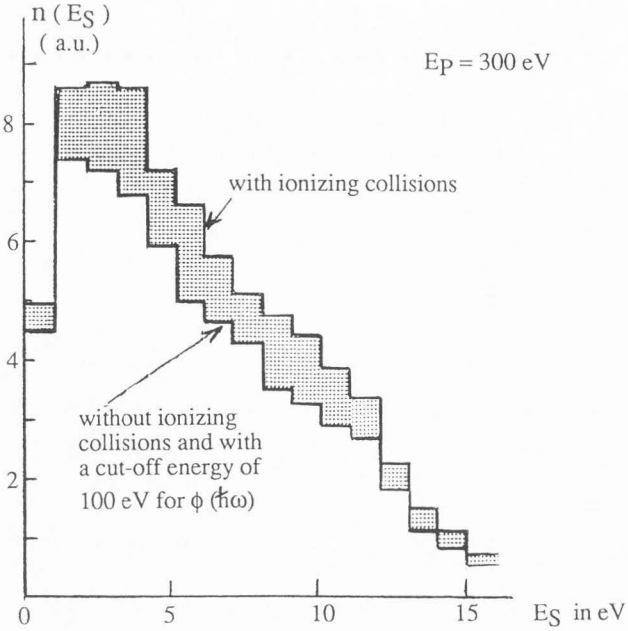

Fig. 19 : Simulated true secondary peak from Al. Contribution of the inner-shell collisions and effect of an energy cut-off (at 100 eV) in the valence band excitation function.

cores. The same question, but to a much lower extent may appear from the introduction of a cut-off energy in the loss function $\phi(\omega)$ associated with the individual inelastic collisions in the Fermi sea. We present in Fig.19 two results showing the influence of both aspects. For an energy of 300 eV, neglecting the inner shell ionizations and allowing a value of 100 eV to the cut-off energy of $\phi(\omega)$ make the value of δ fall from 0.95 to 0.81 and that of η increase from 0.28 to 0.30. The separate influence of the cut-off is to change δ from 0.95 to 0.92 only and to keep η practically unchanged. We can see that the ionizing collisions modify noticeably the true secondary yield and the inelastic backscattering factor. This comes from a direct contribution to the secondary electron emission but also from an indirect contribution due to their high stopping power which tend to limit the penetration of the primary beam in the solid and consequently to locate the secondary electron creation near the surface.

Another question is the precision of the Monte Carlo calculations themselves, owing to the limited size of the statistical sample which necessarily causes fluctuations in the results. To check this point, we have considered for a primary energy of 100 eV, the successive histograms of the secondary peak distribution for statistical samples of 2500, 7500 and 20000 primary electrons. An

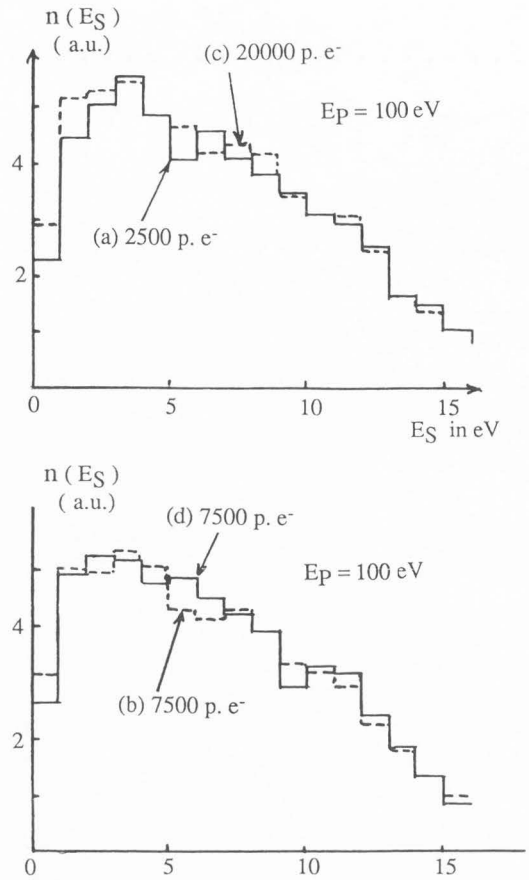

Fig.20 : Simulated true secondary peak from Al. Influence of the statistical sample size. Number of simulated primary electron trajectories : a) 2500 b) and d) 7500 c) 20000. The histograms b) and d) were obtained for two different initializations of the random numbers.

identical initialization of the computed random numbers has been used for these three calculations. From the results shown in Figs.20 a,b and c one can observe the smoothing effect due to the increase of the simulation sample. Roughly speaking, we can estimate that the main features of the distribution are obtained as soon as the sample reaches a value of 7500 primary trajectories. Concerning the yields, the δ values are 0.743, 0.747 and 0.740 for samples of 2500, 7500 and 20000 primary electrons, respectively. The relative fluctuations are thus of the order of 1 % of the final value. For η the respective values are 0.189, 0.183 and 0.182 with fluctuations still of a few per cent. Fig.20d shows the result obtained again for a sample of 7500 primary trajectories, but a different random number sequence due to a different initialization. The yield values we obtained, δ = 0.728 and η = 0.179, are not very far from

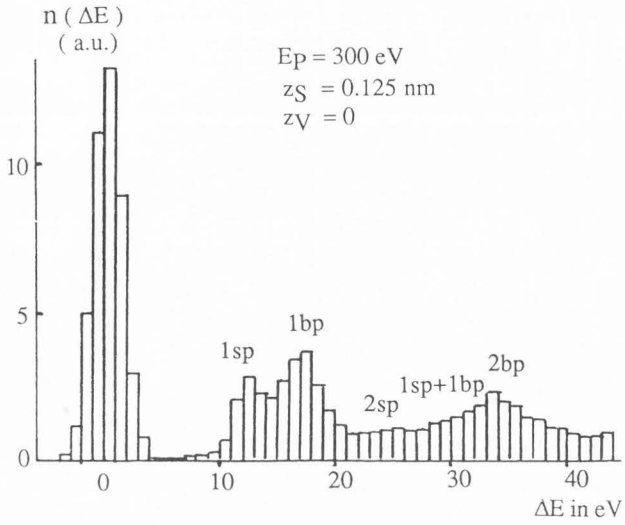

Fig. 21. Simulated energy loss spectrum from Al. The thickness of the surface layer was taken of 0.125 nm.

those calculated with the first sequence. This is an example of the type of precision one can expect in Monte Carlo calculations for a reasonable computer time.

We also present some results for the energy losses in the vicinity of the primary peak. These are shown in Fig.21 for a primary energy of 300 eV. To make a better comparison with the experimental results, the primary electrons have been assumed to have their energies distributed around the mean value E_p according to a normal law with a standard deviation s (here the value s = 1.25 eV has been applied). The energy loss peaks due to one surface plasmon creation (1S) and to one-volume plasmon (1V) are clearly observed at energy loss values of 12 and 16 eV, respectively. Additional structures appear at higher energy losses, which can be attributed to multiple losses such as 2S, 1S+1V, 2V, etc. A very impressive example of such a simulated energy loss spectrum was obtained by Jousset (1987a) for Al, with the layer-by-layer technique.

In our simulation model, as already explained, we have assumed that the surface collective excitations could only take place in a surface domain of a given extension. This step model was introduced by ourselves (see Ganachaud (1977) and Ganachaud and Cailler (1979a,b)) in order to take into account very simply, the results of Feibelman's calculations (1973). According to Feibelman (1973), the free path is reasonably spatially non-varying inside the metal. However, near the surface the bulk plasmon creation rate vanishes but it is compensated by an increase in the surface plasmon rate. Furthermore, Feibelman's calculations showed that the possibility of a surface plasmon creation persisted outside the solid surface which was defined by Feibelman as the surface where the electron density vanishes. The choice of the value of the surface layer thickness is of great importance in order to reproduce the relative heights of the experimental 1S and 1V peaks. Fig.21 is presented for a thickness of 1.25 Å (in the present case, the surface layer is assumed to have a zero extent in the vacuum). The respective heights of the two peaks have been separately calculated by simulation and the ratio h_s/h_b was found to be 0.81, whereas an experimental value of 0.73 was proposed by Roptin. For this ratio, calculated values of 0.45 and 0.90 were found for surface layer thicknesses of 0.75 and 1.75 Å, respectively. This establishes the strong dependence of the plasmon height ratio on the surface layer thickness value. In fact, the thickness of the domain in which the surface collective excitations can be created by a moving electron, varies with the energy of this electron. For primary energies of 100, 300 and 500 eV, we have chosen thickness values of 0.75, 1.25 and 1.75 Å in rough agreement with the energy square root dependence established by Feibelman. The obtained results are exhibited in Figs.22 a,b and c. The corresponding calculated values for the ratio h_s/h_b are respectively of 0.92, 0.81 and 0.67, whereas the experimental values obtained by Roptin were of 1.16, 0.73 and 0.59. Owing to the simplicity of the surface model, this comparison is very encouraging.

Acknowledgments.

The authors thank D. Roptin and J. Pillon for their contribution to the material included in this paper. They wish to thank very sincerely Dr Jorgen Schou for his very attentive and very scrupulous reading of their paper as well as for his numerous and stimulating suggestions. The authors are indebted to Pr. Vicario and Dr. Tholomier for permission to reproduce their results.

References

Adesida I, Shimizu R and Everhart TE (1978). Monte Carlo simulation of electron penetration through thin films of PMMA, Appl. Phys. Lett., **33**, 849-850.

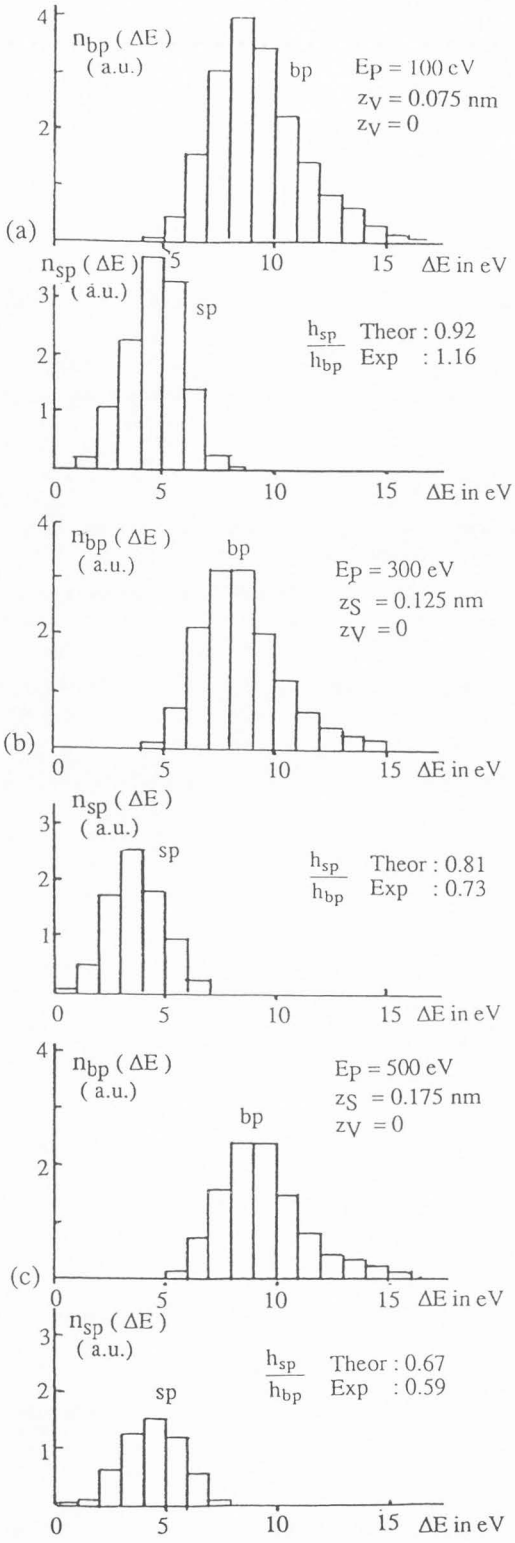

Fig. 22. Simulated energy loss spectrum from Al. Primary electron energy dependence of the one-surface- and the one-bulk-plasmon peaks.

Amelio GF (1970). Theory for the energy distribution of secondary electrons, J. Vac. Sci. Technol., **7**, 593-604.

Ashcroft NW (1966). Electron-ion pseudopotentials in metals, Phys. Lett., **23**, 48-49.

Ashley JC and Tung CJ (1982). Electron inelastic mean free paths in several solids for 200 eV≤E≤10 keV, Surface Interface Anal., **4**, 52

Bennett AJ and Roth LM (1972). Effect of primary electron diffusion on secondary electron emission, Phys. Rev., **B5**, 4309-4324.

Baroody EM (1956). Excitation of electrons in metals by primary electrons, Phys. Rev., **101**, 1679-1684.

Berger MJ, Seltzer SM and Maeda K (1970), Energy deposition by auroral electrons in the atmosphere, J. Atmosph. Terr. Phys., **32**, 1015-1045.

Bindi R, Lanteri H and Rostaing P (1980). A new approach and resolution method of the Boltzmann equation applied to secondary electron emission by reflection for polycristalline Al. J. Phys. D-Appl. Phys., **13**, 267-280.

Bindi R, Lanteri H and Rostaing P (1987). Secondary electron emission induced by electron bombardment of polycristalline metallic targets. Scanning Microscopy, **1**, 1475-1490.

Bonham RA and Strand TG (1963). Analytical expressions for potentials of neutral Thomas-Fermi-Dirac atoms and for the corresponding atomic scattering factors for X-rays and electrons. J. Chem. Phys. **39**, 2200-2204.

Cailler M (1969). Contribution à l'étude théorique de l'émission électronique secondaire induite par bombardement électronique, Thèse d'Etat, Université de Nantes.

Cailler M and Ganachaud JP (1972). Quelques aspects théoriques de l'émission électronique secondaire du cuivre, produite par bombardement d'électrons de faible énergie, J.Physique, **33**, 903-913.

Cailler M. Ganachaud JP and Bourdin JP (1981). The mean free path of an electron in copper between two inelastic collisions, Thin solid films, **75**, 181-189.

Cailler M, Ganachaud JP and Roptin D (1983), Quantitative Auger electron spectroscopy, Adv. Electron. Electron Phys. **61**, 161-298.

Dejardin-Horgues C, Ganachaud JP and Cailler M (1976). A simulation of the transmission of 1 keV electrons through thin films of aluminium, copper and gold, J. Phys. C : Solid State Phys. **9**, L633-L636.

Devooght J, Dubus A. and Dehaes JC (1987). Improved age-diffusion model for low-energy

electron transport in solids. I. Theory, Phys. Rev. **36**, 5093-5109.

Ding ZJ and Shimizu R (1988). Monte-Carlo study of backscattering and secondary electron generation, Surf. Sci., **197**, 539-554.

Ding ZJ and Shimizu R (1989). Inelastic collisions of kV electrons in solids, Surf. Sci., **222**, 313-331.

Doniach S and Sunjic M (1970). Many-electron singularity in X-ray photoemission and X-ray line spectra from metals, J. Phys. C-Solid St. Phys., **3**, 285-291.

Dubot P, Jousset D, Pinet V, Pellerin F and Langeron JP (1988). Simulation of the LMM Auger spectra of copper, Surf. Int. Anal., **12**, 99-104.

Dubus A (1987). Application de méthodes de neutronique au transport d'électrons à basse énergie dans les solides et notamment à l'émission d'électrons secondaires, Thèse d'Etat, Université Libre de Bruxelles.

Dubus A. Devooght J and Dehaes JC (1987). Improved age-diffusion model for low-energy electron transport in solids. II. Application to secondary emission from aluminum, Phys. Rev. **36**, 5110-5119.

Emerson LC. Birkhoff RD. Anderson VE and Ritchie RH (1973). Electron slowing-down spectrum in irradiated silicon, Phys. Rev. **B7**, 1798-1811.

Feibelman PJ (1973). Spatial variation of the electron mean free path near a surface, Surf. Sci., **36**, 558-568.

Fitting HJ and Reinhardt J (1985). Monte Carlo simulation of keV-electron scattering in solid targets, Phys. Stat. Sol. (a), **88**, 245-259.

Ganachaud JP and Cailler M (1973a). Traitement unifié de l'émission électronique secondaire du cuivre par une méthode de Monte-Carlo, J. Physique, **34**, 91-98.

Ganachaud JP and Cailler M (1973b). Description d'un modèle d'émission électronique secondaire prenant en compte collisions élastiques et inélastiques, C. R. Acad. Sc. Paris, **276**, 543-546.

Ganachaud JP (1977). Contribution à l'étude théorique de l'émission électronique secondaire des métaux, Thèse d'Etat, Université de Nantes.

Ganachaud JP. and Cailler M (1979 a), A Monte-Carlo calculation of the secondary electron emission of normal metals. I. The model, Surf. Sci. **83**, 498-518.

Ganachaud JP. and Cailler M (1979 b), A Monte-Carlo calculation of the secondary electron emission of normal metals. II. Results for aluminium, Surf. Sci. **83**, 519-530.

Goto K, Ishikawa K, Koshikawa T and Shimizu R (1975). Auger and secondary electrons excited by backscattered electrons; an approach to quantitative analysis, Surf. Sci., **47**, 477-494.

Gryzinski M (1965 a). Two-particle collisions. I. General relations for collisions in the laboratory system of coordinates, Phys. Rev. **138**, A322-A335.

Gryzinski M (1965 b). Two-particle collisions. II. Coulomb collisions in the laboratory system, Phys. Rev. **138**, A305-A321.

Gryzinski M (1965 c). Classical theory of atomic collisions. I. Theory of inelastic collisions, Phys. Rev. **138**, A336-A358.

Hachenberg O and Brauer W (1959). Secondary electron emission from solids, Adv. Electron. Electron. Phys. **11**, 413-499.

Heine V (1970). The pseudopotential concept, Solid State Phys., Acad. Press N.Y, **24**, 1-36.

Ichimura S and Shimizu R (1981). Backscattering correction for quantitative Auger analysis. I. Monte Carlo calculations of backscattering factors for standard materials, Surf. Sci. **112**, 386-408.

Jablonski A (1985). Elastic backscattering of electrons from surfaces, Surf. Sci., **151**, 166-182.

Jablonski A, Gryko J, Kraaer J and Tougaard S (1989). Elastic electron backscattering from surfaces, Phys. Rev., **B 39**, 61-71.

Jousset D (1987a). Etude théorique et expérimentale des distributions énergétiques des électrons primaires, secondaires et Auger rétrodiffusés en spectroscopie des électrons Auger. Application à la caractérisation des couches minces d'alumine sur aluminium. Thèse Docteur es-Sciences, Université de Paris 6.

Jousset D, Dubot P, Langeron JP and Villatte M (1987b). AES characterization of Al_2O_3 thin films on Al. Proc. International Symposium on trends and new applications in thin films, Strasbourg, and Le Vide, les couches minces, **235** suppl., 629-634.

Jousset D, Dubot P and Langeron JP (1987c). Experimental and theoretical determination of the aluminium KLL Auger peaks areas. Correlation with the thickness of Al_2O_3 films on Al, 2d Nordic Conf. on Surf. Sci., Linköping.

Jousset D and Langeron JP (1987d). Energy distribution of primary backscattered electrons in Auger electron spectroscopy, J. Vac. Sci. Technol. **A 5**, 989-995.

Koshikawa T and Shimizu R (1974). A Monte-Carlo calculation of low-energy secondary electron emission from metals. J. Phys. D : Appl. Phys., **7**, 1303-1315.

Kotera M (1990). A simulation of secondary electron trajectories in solids, Scanning

Microscopy, Supplement 4, 111-126.

Lanteri H. Bindi R. and Rostaing P (1980). Modèle théorique de la rétrodiffusion d'électrons par des cibles massives d'aluminium, d'argent et de cuivre, J. Phys. D : Appl. Phys., **13**, 677-692.

Lanteri H. Bindi R. and Rostaing P (1981). Application of splitting-up method to the numerical treatment of transport equation- Analysis of the transmission of electrons through thin self supporting metallic targets, J. Comput. Phys., **39**, 22-45.

Lanteri H. Bindi R. and Rostaing P (1982). Modèle théorique de la transmission et de la rétrodiffusion d'électrons dans des cibles métalliques minces ou semi-infinies : Application à l'aluminium, l'argent et le cuivre, Thin Solid films, **88**, 309-333.

Lanteri H. Bindi R. and Rostaing P (1986). Modèle théorique de la transmission et de la rétrodiffusion d'électrons dans des cibles métalliques minces ou semi-infinies : II Application à l'étude des pertes caractéristiques des électrons transmis et rétrodiffusés dans le cas de l'aluminium, Thin Solid films, **135**, 289-299.

Lanteri H. Bindi R. and Rostaing P (1988). Transport models for backscattering and transmission of low-energy (<3 kilovolts) electrons from solids, Scanning Microscopy, **2**, 1927-1945.

Lindhard J (1954). On the properties of a gas of charged particles, Kgl. Danske Videnskab. Selskab, Mat. Fys. Medd. **28**, 1-57.

Manson ST (1972). Inelastic collisions of fast charged particles with atoms : Ionization of the Aluminum L shell, Phys. Rev., **A6**, 1013-1024.

Mignot H (1974). Extension à l'or et à l'argent d'un modèle théorique de simulation de l'émission électronique secondaire induite par bombardement électronique. Thèse de Spécialité (3ème cycle), Université de Nantes.

Moulin B, Ganachaud JP and Cailler M (1973). Considérations sur l'importance de quelques hypothèses physiques dans la théorie de l'émission électronique secondaire, Phys. Stat. Sol., **59**, 79-

Nagel SR and Witten TA (1975) Local field effects on inelastic electron scattering, Phys. Rev., **B11**, 1623-1635.

Nigam BP, Sundaresan MK and Wu T-Y (1959). Theory of multiple scattering : Second Born Approximation and corrections to Moliere's work, Phys. Rev., **115**, 491-502.

Pendry JB (1974). Low energy electron diffraction, Acad. Press, London and New-York.

Penn DR (1976) Electron mean free paths for free-electron-like materials, Phys. Rev. **B13**, 5248-5254.

Penn DR (1987). Electron mean-free-path calculations using a model dielectric function, Phys. Rev., **B35**, 482-486.

Pillon J, Roptin D and Cailler M (1976). Secondary electron emission from aluminium, Surf. Sci., **59**, 741-748.

Pillon J, Ganachaud JP, Roptin D, Mignot H, Dejardin-Horgues C and Cailler M (1977). Secondary electron emission of metal surface (Al, Ag, Au), Proc. 7th Intern. Vac. Conf. & 3rd Intern. Conf. Solid Surfaces (Vienna), 473-476.

Powell CJ (1976). Cross-sections for ionization of inner-shell electrons by electrons, Rev. Mod. Phys., **48**, 33-47.

Puff H (1964). Zur theorie der sekundärelektronenemission. Der transportprozess, Phys. Stat. Sol. **4**, 125-365.

Quinn JJ (1962). Range of excited electrons in metals, Phys. Rev., **126**, 1453-1457.

Raether H (1965). Solid state excitations by electrons, in Springer tracts in modern physics, ed. Höhler G. (Springer, New york) **38**.

Ritchie RH. Garber FW. Nakai MY. Birkhoff RD (1969). Low energy electron mean free paths in solid, Adv. Radiat. Biol., **3**, 1-28.

Ritchie RH. Tung CJ. Anderson VE and Ashley JC (1975). Electron slowing-down spectra in solids, Radiat. Res. **64**, 181-204.

Ritchie RH and Howie A (1977). Electron excitation and the optical potential in electron microscopy, Phil. Mag., **36**, 463-481.

Roptin D (1975). Etude expérimentale de l'émission électronique secondaire de l'aluminium et de l'argent. Thèse de Docteur-Ingénieur, ENSM et Université de Nantes.

Rösler M and Brauer W (1981a). Theory of secondary electron emission. I. General theory for nearly-free-electron metals, Phys. Stat. Sol. (b) **104**, 161-175.

Rösler M and Brauer W (1981b). Theory of secondary electron emission. II. Application to aluminum, Phys. Stat. Sol. (b) **104**, 161-175.

Rösler M and Brauer W (1988). Theory of electron emission from solids by proton and electron bombardment, Phys. Stat. Sol. (b) **148**, 213-226.

Schiff LI (1955) Quantum mechanics, Mc Graw-Hill book Co, New-York, (cf p.170).

Schou J (1980a). Transport theory for kinetic emission of secondary electrons from solids, Phys. Rev., B **22**, 2141-2174.

Schou J (1980b). Transport theory for kinetic emission of secondary electrons from solids by electron and ion bombardment, Nucl. Instr. Meth., **170**, 317-320.

Schou J (1988). Secondary electron emission from solids by electron and proton bombardment, Scanning Microscopy, **2**, 607-632.

Shimizu R, Honji M and Murata K (1970). Investigation of energy dissipation of electrons in Al- and Cu-targets by Monte-Carlo method, Jap. J. appl. Phys., **9**, 1291-1296.

Shimizu R, Ikuta T and Murata K (1972). The Monte Carlo technique as applied to the fundamentals of EPMA and SEM, J.Appl.Phys., **43**, 4233-4249.

Shimizu R, Kataoka Y, Matsukawa T, Ikuta T, Murata K and Hashimoto H (1975). Energy distribution measurement of transmitted electrons and Monte Carlo simulation for kilovolt electron, J. Phys.D : Appl. Phys., **8**, 820-828.

Shimizu R, Kataoka Y, Ikuta T, Kosikawa T and Hashimoto H (1976). A Monte Carlo approach to the direct simulation of electron penetration in solids, J. Phys.D : Appl. Phys., **9**, 101-114.

Shimizu R and Everhart TE (1978). A semiempirical stopping-power formula for use in microprobe analysis, Appl. Phys. Lett. **33**, 784-786.

Shimizu R and Ichimura S. (1981a). Application of Monte Carlo technique to quantitative Auger analysis- An approach for quantitative correction of electron backscattering effect, Scanning Electron Microscopy/ **I**, 1981, 221-230.

Shimizu R. and Ichimura S (1981b). Quantitative analysis by Auger electron spectroscopy-Monte Carlo calculations of electron backscattering effects, Technical Reports Toyota Foundation No.**I-006,76-0175** (copy available from R. Shimizu).

Shimizu R. and Ichimura S (1983). Direct Monte Carlo simulation of scattering processes of kV electron in aluminum; Comparison of theoretical N(E) spectra with experiment, Surf. Sci. **133**, 250-266.

Shimizu R. and Ichimura S (1984). Direct Monte Carlo simulation of kV electron scattering processes- N(E) spectra for aluminum, in : Electron beam interactions with solids, D.F. Kyser, D.E. Newbury, H. Niedrig, R. Shimizu (eds.), SEM, Inc., AMF O'Hare, Il 60666, 165-172.

Sickafus EN (1977a). Linearized secondary-electron cascades from the surfaces of metals. I. Clean surfaces of homogeneous specimens, Phys. Rev. **B16**, 1436-1447.

Sickafus EN (1977b). Linearized secondary-electron cascades from the surfaces of metals. II. Surface and subsurface sources , Phys. Rev. **B16**, 1448-1458.

Smrcka L (1970). Energy band-structure of aluminium by the augmented-plane-wave method, Czech. J. Phys., **B 20**, 291-300.

Stolz H. (1959) Zur theorie der Sekundärelektronenemission von Metallen. Der transportprocess, Ann. Phys. **3**, 197-210.

Streitwolf HW (1959). Zur theorie der sekundärelektronen-emission von metallen der anregungsprozess, Ann. Phys. **3**, 183-196.

Tanuma S, Powell CJ and Penn DR (1988). Calculations of electron inelastic mean free paths for 31 materials, Surf. Interf. Anal., **11**, 577-589.

Tholomier M, Vicario E and Doghmane N. (1987). Simulation par la méthode de Monte Carlo de l'influence des électrons rétrodiffusés en spectrométrie d'électrons Auger. Ière partie. J. Microsc. Spectrosc. Electron., **12**, 449-460.

Tholomier M, Vicario E and Doghmane N. (1988). Simulation par la méthode de Monte Carlo de l'influence des électrons rétrodiffusés en spectrométrie d'électrons Auger. 2ème partie. J. Microsc. Spectrosc. Electron., **13**, 119-133.

Thomas S and Pattinson EB (1970). Range of electrons and contribution of backscattered electrons in secondary production in aluminium, J. Phys. D, **3**, 349-357.

Tung CJ and Ritchie RH (1977). Electron slowing-down spectra in aluminum metal, Phys. Rev. **B16**, 4302-4313.

Valkealahti S and Nieminen RM (1983). Monte-Carlo calculations of keV electron and positron slowing down in solids, Appl. Phys., **A32**, 95-106.

Valkealahti S and Nieminen RM (1984). Monte-Carlo calculations of keV electron and positron slowing down in solids. II, Appl. Phys., **A 35**, 51-59.

Valkealahti S, Schou J and Nieminen RM (1989). Energy deposition of keV electrons in light elements, J. Appl. Phys., **65**, 2258-2266.

Werner U and Heydenreich J (1984). A simple Monte Carlo simulation of the electron-target interaction on the basis of an empirical scattering formula, Ultramicroscopy, **15**, 17-28.

Wolff PA (1954). Theory of secondary electron cascade in metals, Phys. Rev., **95**, 56-66.

Discussion with Reviewers

J. Schou : In view of the accuracy of the Monte Carlo simulations, I do not see any major differences between the three figures in Fig.17. Is it possible for the authors on the basis of these results or other results to give any statement of the relative contribution of the different modes of plasmon decay?

Authors : The differences between the three figures in Fig. 17 are effectively rather small and are the most easily observed from a comparison with the experimental results. A complementary information can be found in Ganachaud's thesis (1977) or in a paper by Ganachaud and Cailler (1979b) where separate contributions of the bulk plasmon damping modes and the surface plasmon damping can be found. It was suggested that the bulk plasmon damping processes were all competitive and that the surface plasmon damping contributes only weakly to the yield. In fact, we were left with the question of evaluating the relative contributions of the different possible mechanisms (one-pair, two-pair, multi-pair processes, inter-band effects) to the bulk and the surface plasmon damping? Up to now, this question has not received a definite answer and there is a need for supplementary experimental studies. However, we want to emphasize the very interesting theoretical work performed by Rösler and Brauer (1981a,b, 1988) to evaluate the bulk plasmon damping rate via interband transitions and the contribution of this mechanism to the secondary electron emission.

M. Kotera : The differential cross section for elastic scattering of electrons you used in the simulation (Cailler and Ganachaud, SEM, 1, 85-97 (1983)) is obtained from the Schrödinger equation. The cross section Ichimura and Shimizu (Surf. Sci., 112, 386-408 (1981)), Reimer and Krefting (NBS Spec. Publ. 460, 45-60 (1976), and Kotera (J. Appl. Phys., 65, 3391-3398 (1989)) used is obtained from the Dirac equation. Can you evaluate the difference between these two cross sections in the angular dependence and the energy dependence for various elemrents?

Authors : We have no direct experiment of such effects. Relativistic effects have to be taken into account for a correct description of the potential in rather heavy materials or for high velocity incident particles. In the case of an Al target and for the energies we considered, such relastivistic effects are likely negligible.

R.H. Ritchie : You have indicated that, in your calculations of secondary electron emission from solids, you have used elastic scattering mean free paths computed assuming independent (binary) scattering of the electron on individual atoms (or ions) in the solid. Since in a crystal, an electron in a Bloch state can scatter only on disorder, defects, or impurities in the crystal, would it not be more appropriate to use, e.g., phonon scattering mean free paths in your calculations ?

Authors : Two main assumptions are required to introduce the Bloch wave functions. The first one is the Born-Oppenheimer approximation which assumes that the nuclei move so slowly compared with the electrons, this makes it possible to deal with the electronic and nuclear motions separately. The second one considers that the potential energy of an electron moving in the crystal will have the same periodicity as the lattice and is not time-dependent. In other words, in quantum mechanics, the propagation of an electron in a crystal results from interferences between the waves diffused by all the nuclei. Such an assumption is justified in the absence of inelastic collisions, that is for an electron in a given stationnary state, for instance for an electron having an energy less than the Fermi level. For electrons having an energy just above the Fermi level, the assumptions are still rather well justified. However, the moving particles have to be described as wave packets and have collisions with the lattice irregularities, and this is the reason for the electrical resistance of the solid. For electrons of high energies, the inelastic effects are so high that the assumption of a non-time dependent and periodical potential is no longer justified. This is particularly true when the inelastic mean free path has low values and that the incident particle strongly polarizes the surrounding medium.